Probes of
extended dark matter structures

Djuna Lize Croon (IPPP Durham)
Catch22+2, May 2024
djuna.l.croon@durham.ac.uk | djunacroon.com

Dark matter substructure

Two things we may agree upon…

- All of our evidence for Dark Matter is gravitational
- Many dark matter models feature substructure

PBHs

Boson stars

Subhalos

Miniclusters

Mirror stars

Image credit: Adam Rogers, theamateurrealist.wordpress.com

Dark matter substructure

Two things we may agree upon…

- All of our evidence for Dark Matter is gravitational
- Many dark matter models feature substructure

PBHs | Boson stars | Subhalos | Miniclusters | Mirror stars

- Microlensing can be used to probe such models

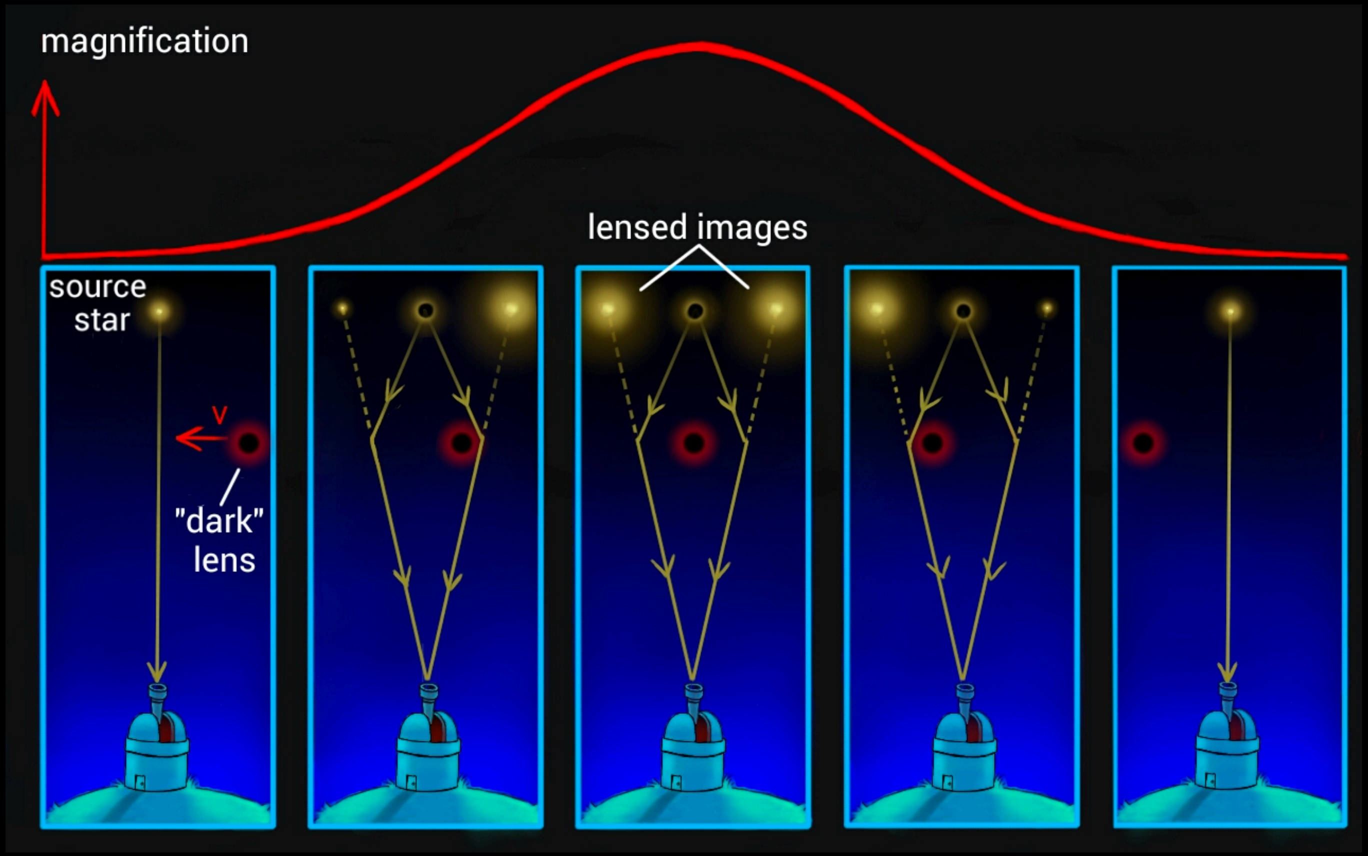

Image credit: Adam Rogers, theamateurrealist.wordpress.com

Geometry

"Thin screen approximation"

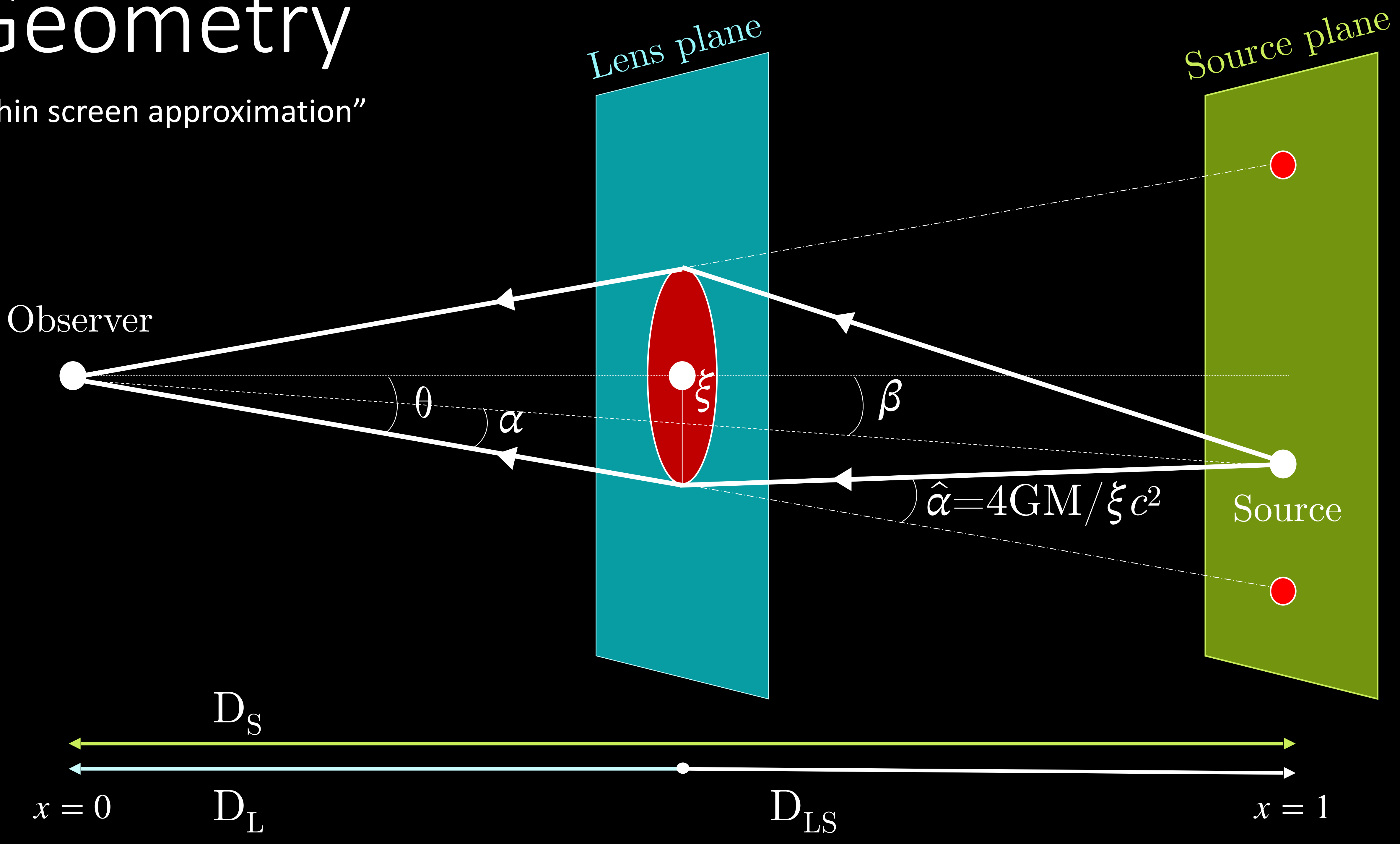

Geometry

"Thin screen approximation"

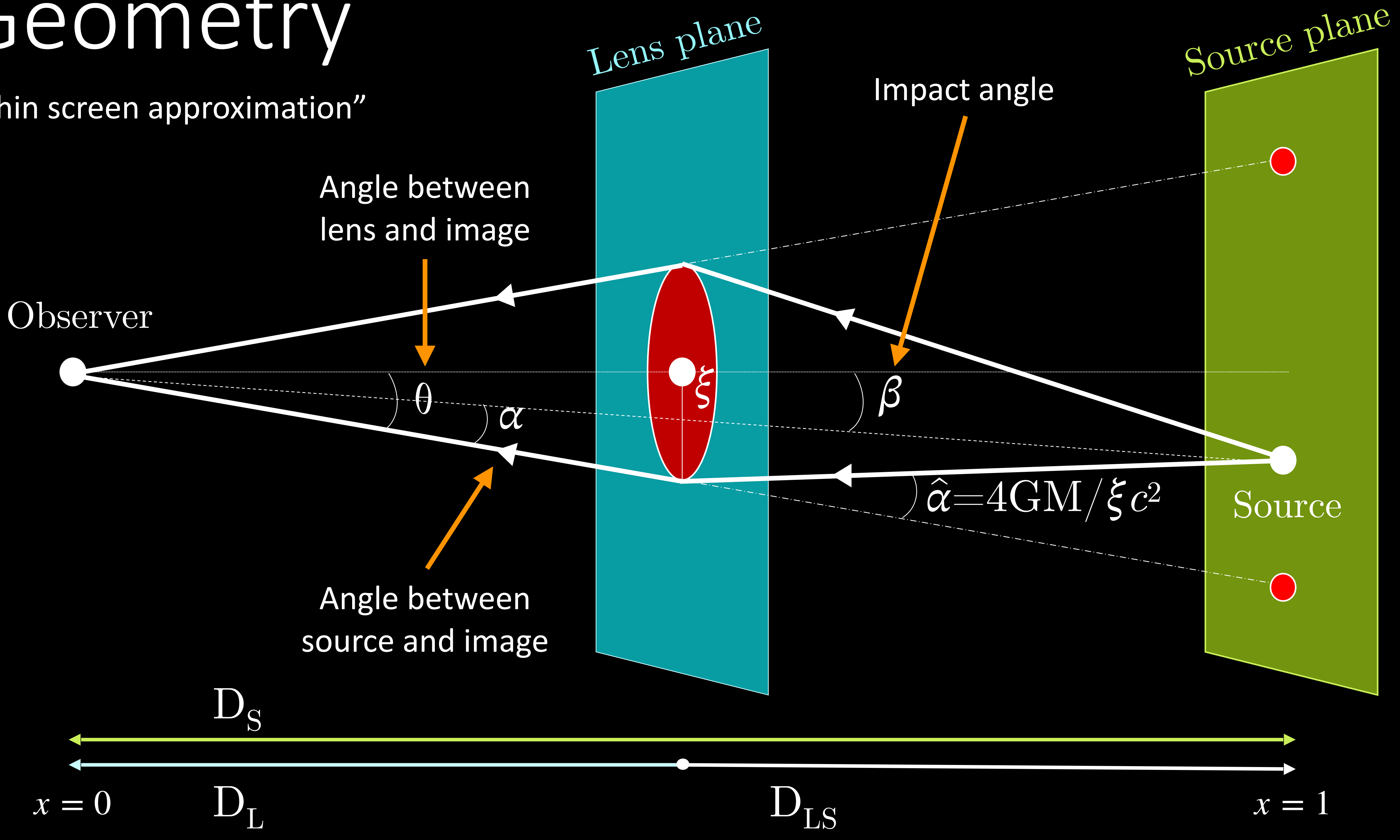

Geometry

“Thin screen approximation”

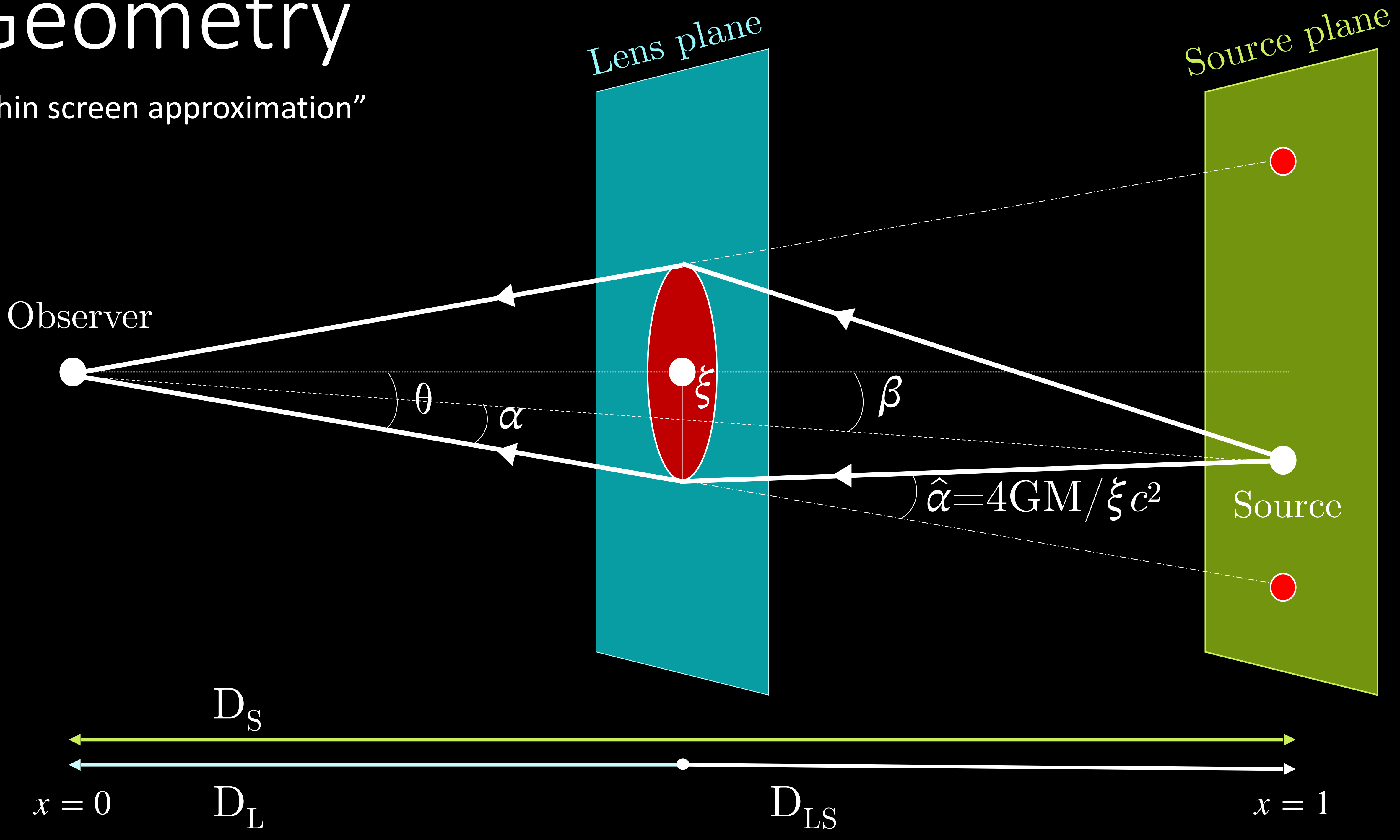

$$\theta D_S = \beta D_S - \hat{\alpha} D_{LS} \rightarrow \underbrace{\beta = \theta - \alpha = \theta - \hat{\alpha}\frac{D_{LS}}{D_S} = \theta - \frac{4GM(\theta)}{\theta c^2}\frac{D_{LS}}{D_S}}_{\text{Lensing equation}}$$

Geometry

"Thin screen approximation"

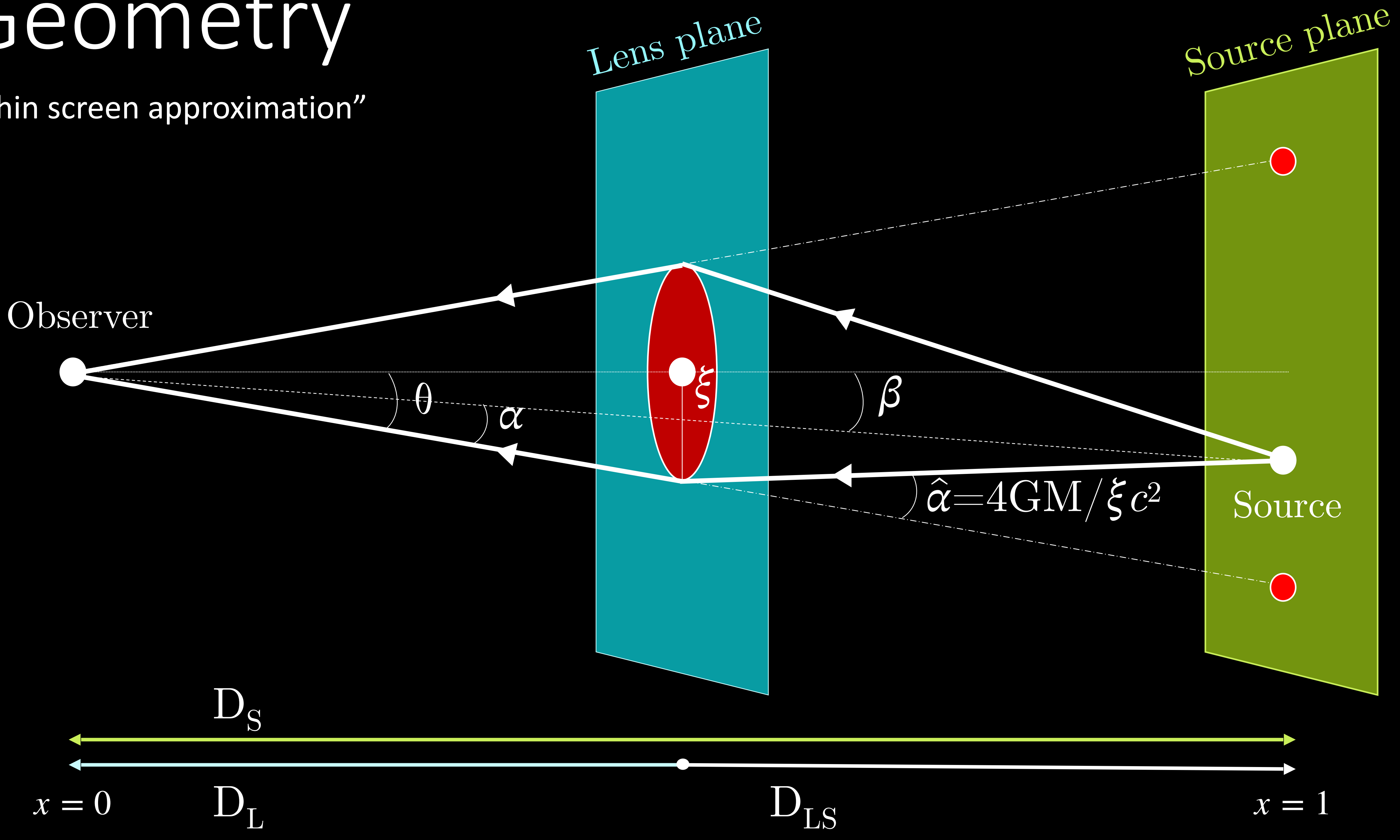

$$\theta D_S = \beta D_S - \hat{\alpha} D_{LS} \rightarrow \beta = \theta - \alpha = \theta - \hat{\alpha}\frac{D_{LS}}{D_S} = \theta - \frac{4GM(\theta)}{\theta c^2}\frac{D_{LS}}{D_S}$$

$$\beta = 0 \rightarrow , \theta \equiv \theta_E = \sqrt{\frac{4GM}{c^2}\frac{D_{LS}}{D_L D_S}}$$

Einstein radius

$r_E = \theta_E D_L$

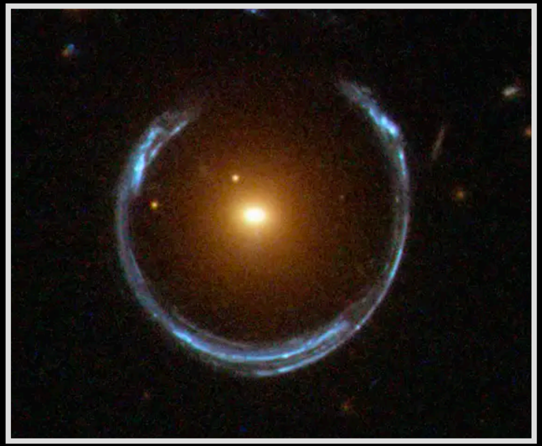

Near perfect Einstein Ring with the HST

The lensing tube

- Magnification: $\mu = \frac{\theta}{\beta}\frac{d\theta}{d\beta} = \sum \mu_i$

The lensing tube

- Magnification: $\mu = \frac{\theta}{\beta}\frac{d\theta}{d\beta} = \sum \mu_i \underset{\substack{\uparrow \\ \text{point-like lens}}}{=} \frac{\overset{\substack{\text{normalised impact parameter } u \equiv \beta/\theta_E \\ \downarrow}}{u}{}^2 + 2}{u\sqrt{u^2+4}} \underset{\substack{\uparrow \\ u \to 1}}{\rightarrow} 1.34$

The lensing tube

normalised impact parameter $u \equiv \beta/\theta_E$

- Magnification: $\mu = \frac{\theta}{\beta}\frac{d\theta}{d\beta} = \sum \mu_i = \frac{u^2+2}{u\sqrt{u^2+4}} \rightarrow 1.34$

point-like lens

$u \rightarrow 1$

- θ_E defines a lensing tube with radius $r_E = \theta_E D_L$
- Defining $\tau \equiv \theta/\theta_E$, $m(\tau) \equiv M(\theta_E \tau)/M$,

$$u = \tau - \frac{m(\tau)}{\tau} \quad \text{with} \quad \mu = \left|1 - \frac{m(\tau)}{\tau^2}\right|^{-1} \left|1 + \frac{m(\tau)}{t^2} - \frac{1}{\tau}\frac{dm(\tau)}{d\tau}\right|^{-1}$$

DC, D. McKeen, N. Raj, PRD, arXiv:2002.08962 [astro-ph.CO]

The lensing tube

normalised impact parameter $u \equiv \beta/\theta_E$

- Magnification: $\mu = \frac{\theta}{\beta}\frac{d\theta}{d\beta} = \sum \mu_i = \frac{u^2+2}{u\sqrt{u^2+4}} \to 1.34$

point-like lens

$u \to 1$

- θ_E defines a lensing tube with radius $r_E = \theta_E D_L$
- Defining $\tau \equiv \theta/\theta_E$, $m(\tau) \equiv M(\theta_E \tau)/M$,

$$u = \tau - \frac{m(\tau)}{\tau} \quad \text{with} \quad \mu = \left|1 - \frac{m(\tau)}{\tau^2}\right|^{-1} \left|1 + \frac{m(\tau)}{t^2} - \frac{1}{\tau}\frac{dm(\tau)}{d\tau}\right|^{-1}$$

Projected lens mass distribution

$$m(\tau) \equiv M(\theta_E \tau)/M = \frac{\int_0^\tau d\sigma\sigma \int_0^\infty d\lambda\, \rho(r_E\sqrt{\sigma^2+\lambda^2})}{\int_0^\infty d\gamma \gamma^2 \rho(r_E \gamma)}$$

DC, D. McKeen, N. Raj, PRD, arXiv:2002.08962 [astro-ph.CO]

The lensing tube

normalised impact parameter $u \equiv \beta/\theta_E$

- Magnification: $\mu = \frac{\theta}{\beta}\frac{d\theta}{d\beta} = \sum \mu_i = \frac{u^2+2}{u\sqrt{u^2+4}} \rightarrow 1.34$

point-like lens

$u \rightarrow 1$

- θ_E defines a lensing tube with radius $r_E = \theta_E D_L$
- Defining $\tau \equiv \theta/\theta_E$, $m(\tau) \equiv M(\theta_E \tau)/M$,

$$u = \tau - \frac{m(\tau)}{\tau} \quad \text{with} \quad \mu = \left|1 - \frac{m(\tau)}{\tau^2}\right|^{-1} \left|1 + \frac{m(\tau)}{t^2} - \frac{1}{\tau}\frac{dm(\tau)}{d\tau}\right|^{-1}$$

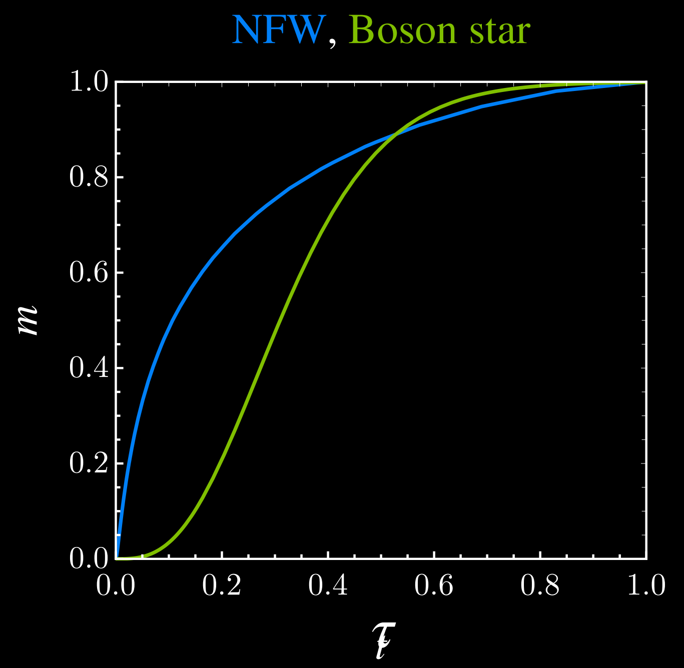

$$m(\tau) \equiv M(\theta_E \tau)/M = \frac{\int_0^\tau d\sigma \sigma \int_0^\infty d\lambda\, \rho(r_E\sqrt{\sigma^2+\lambda^2})}{\int_0^\infty d\gamma \gamma^2 \rho(r_E \gamma)}$$

DC, D. McKeen, N. Raj, PRD, arXiv:2002.08962 [astro-ph.CO]

Threshold impact parameter

Define $u_{1.34}$ *by* $\mu_{\rm tot}(u \le u_{1.34}) > 1.34$

All smaller impact parameters produce a magnification above $\mu > 1.34$

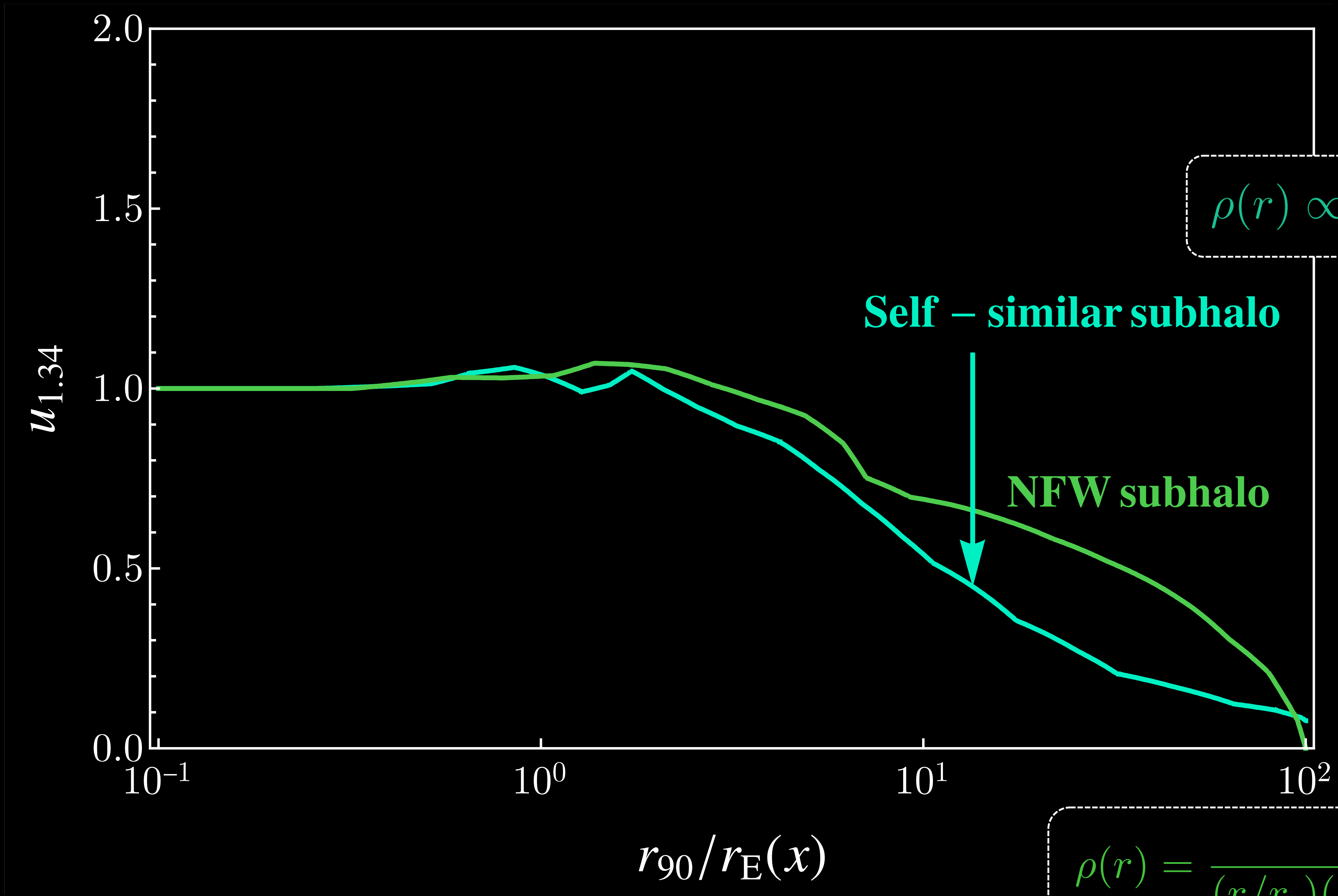

$\rho(r) \propto r^{-9/4}$

$$\rho(r) = \frac{\rho_{\rm s}}{(r/r_{\rm s})(1+r/r_{\rm s})^2}$$

DC, D. McKeen, N. Raj, PRD, arXiv:2002.08962 [astro-ph.CO]

Threshold impact parameter

Define $u_{1.34}$ *by* $\mu_{\rm tot}(u \le u_{1.34}) > 1.34$

All smaller impact parameters produce a magnification above $\mu > 1.34$

Numerically solve the Schrodinger-Poisson equations

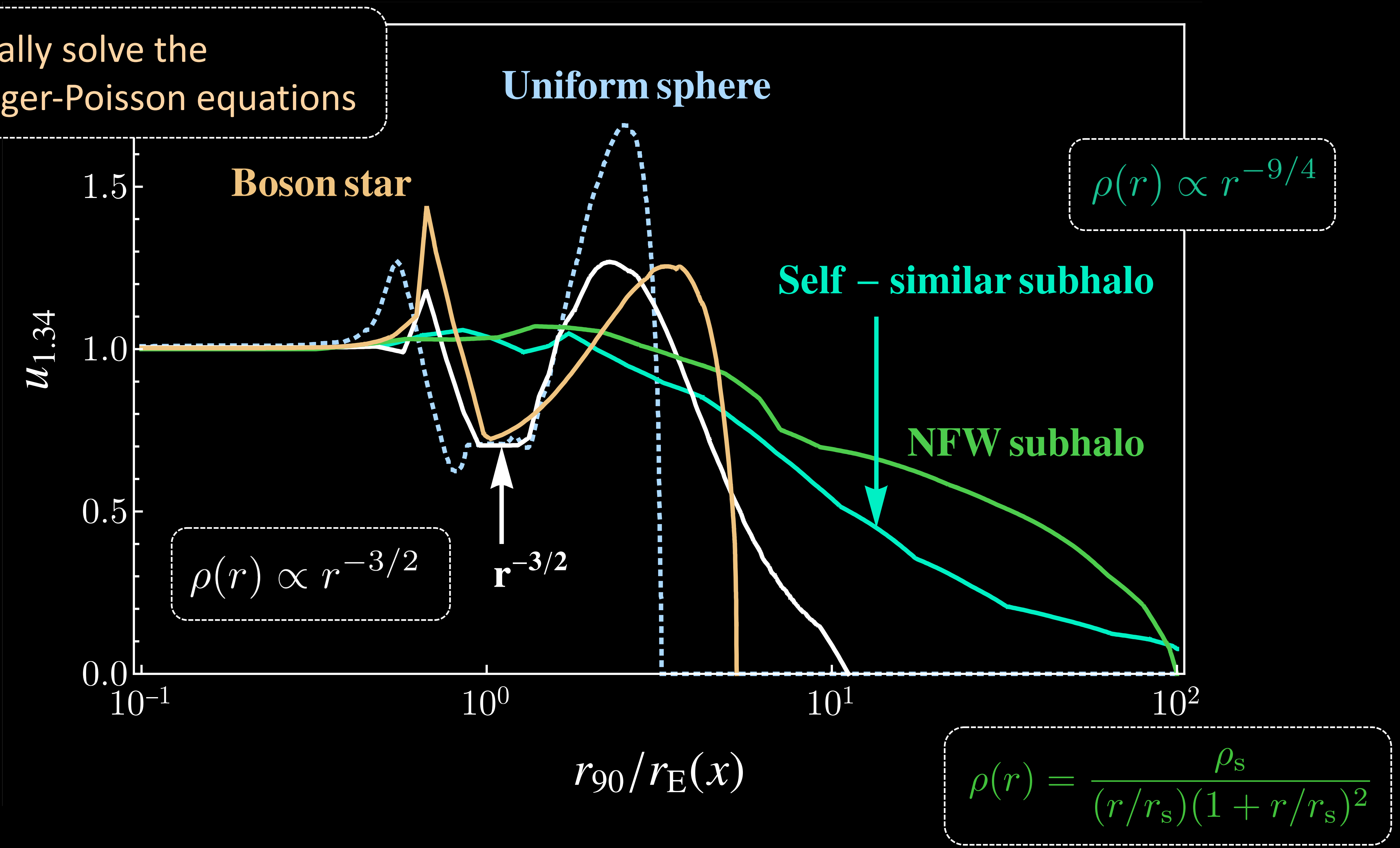

DC, D. McKeen, N. Raj, PRD, arXiv:2002.08962 [astro-ph.CO]

Constraints on DM fraction

Generally, constraints on extended objects are weaker…

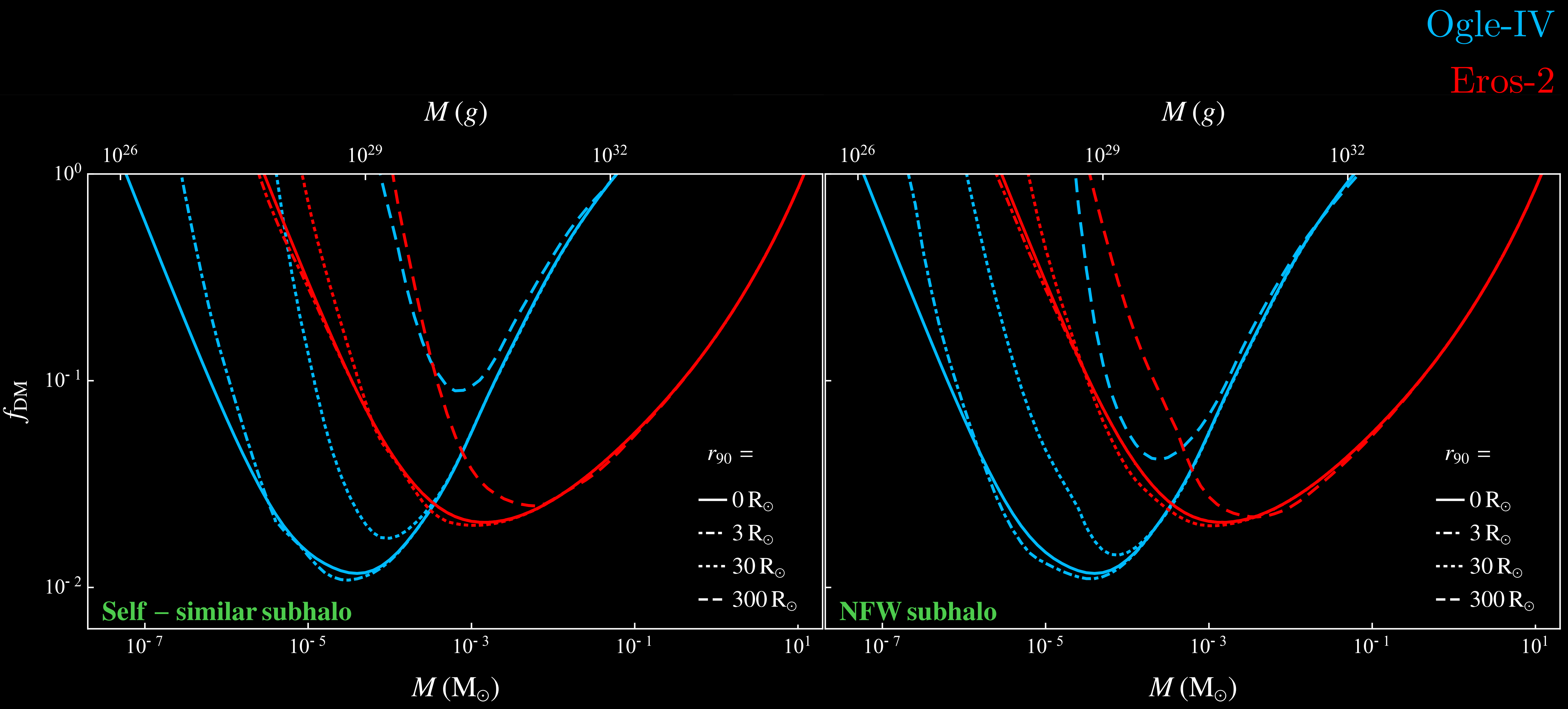

DC, D. McKeen, N. Raj, PRD, arXiv:2002.08962 [astro-ph.CO]

Constraints on DM fraction

But for sufficiently flat density profiles, caustics change the constraints

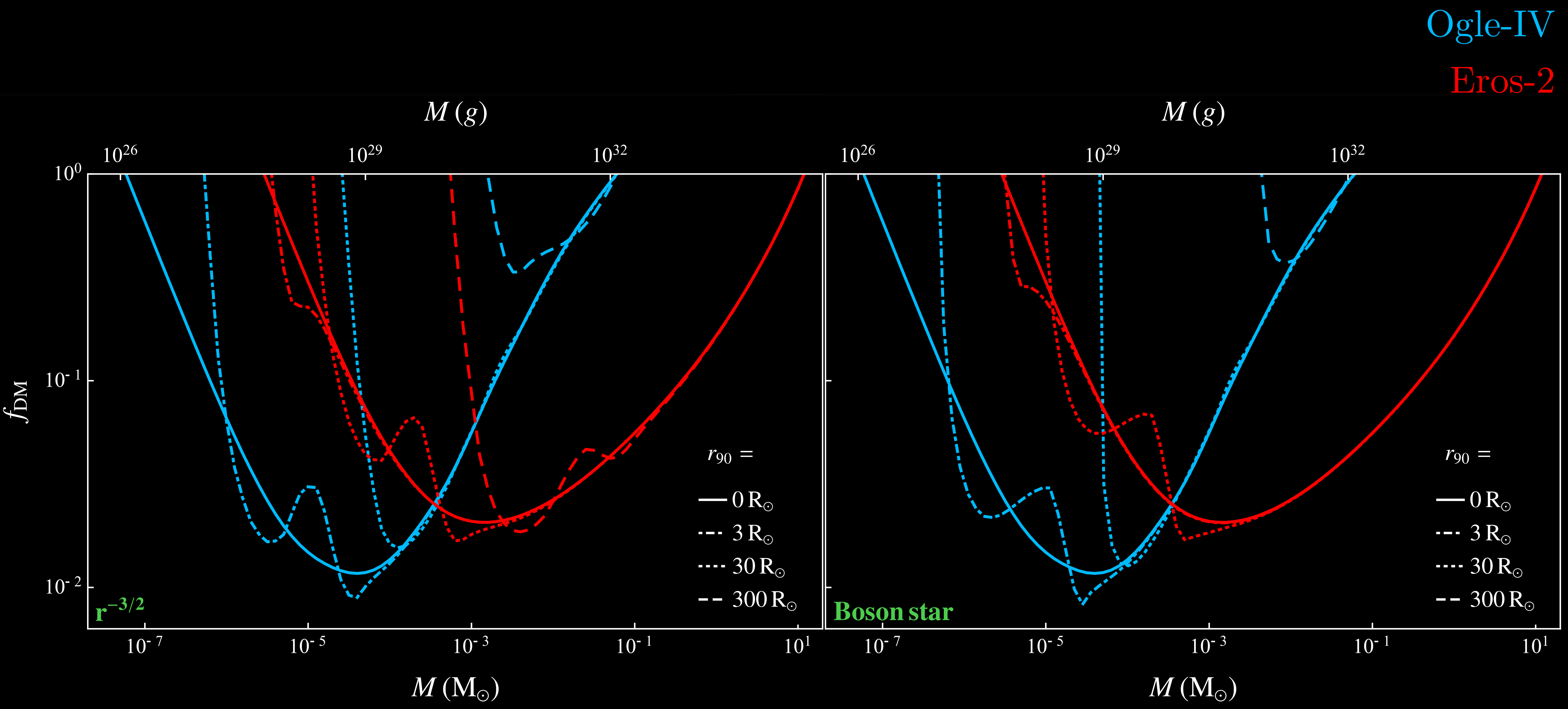

DC, D. McKeen, N. Raj, PRD, arXiv:2002.08962 [astro-ph.CO]

Extended sources: $r_E = \theta_E D_L \sim r_S$

Same procedure as before, but now $u_{1.34}$ is a function of both r_{90} and r_S

DC, D. McKeen, N. Raj, Z. Wang, PRD, arXiv:2007.12697 [astro-ph.CO]

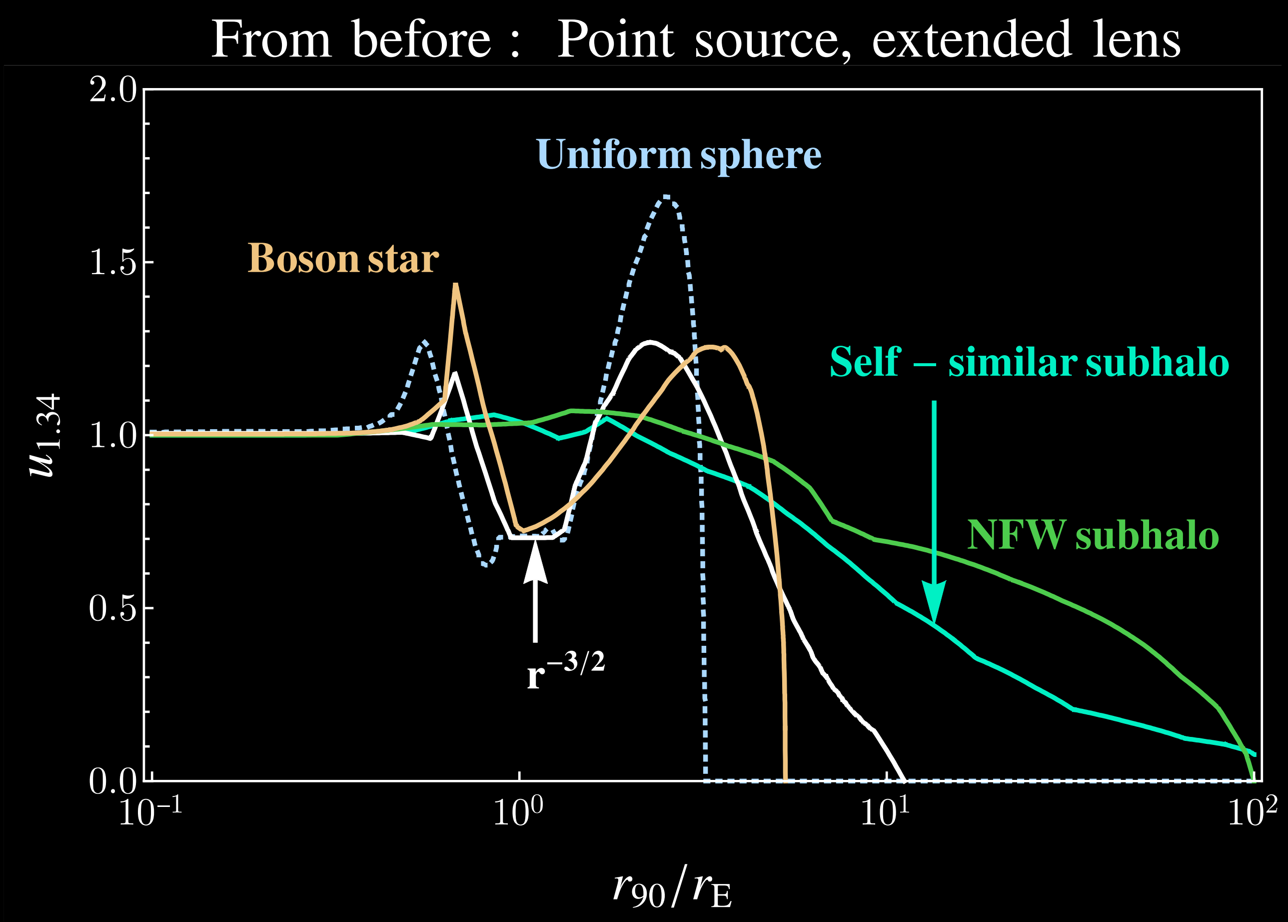

Extended sources: $r_E = \theta_E D_L \sim r_S$

Same procedure as before, but now $u_{1.34}$ is a function of both r_{90} and r_S

DC, D. McKeen, N. Raj, Z. Wang, PRD, arXiv:2007.12697 [astro-ph.CO]

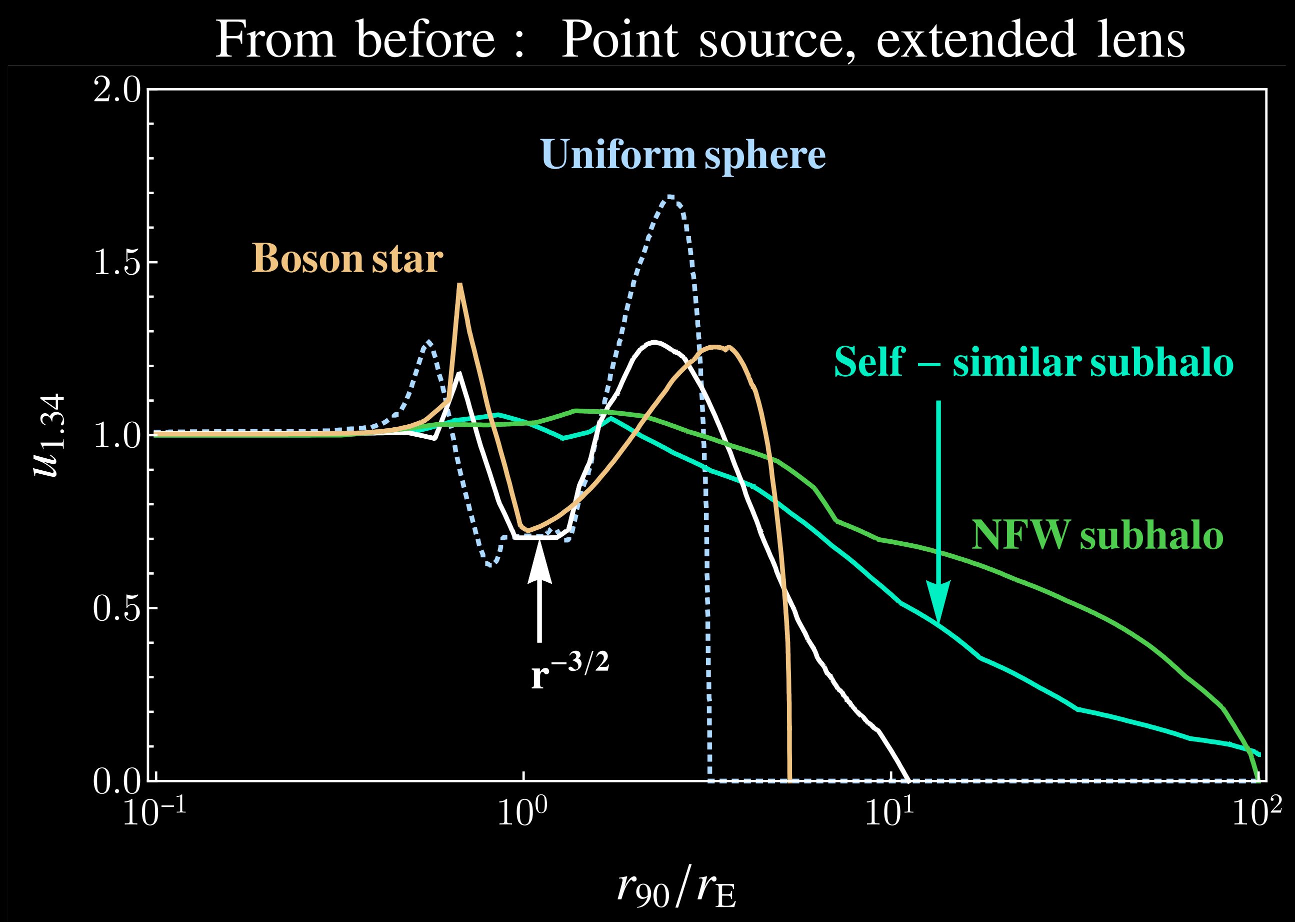

+

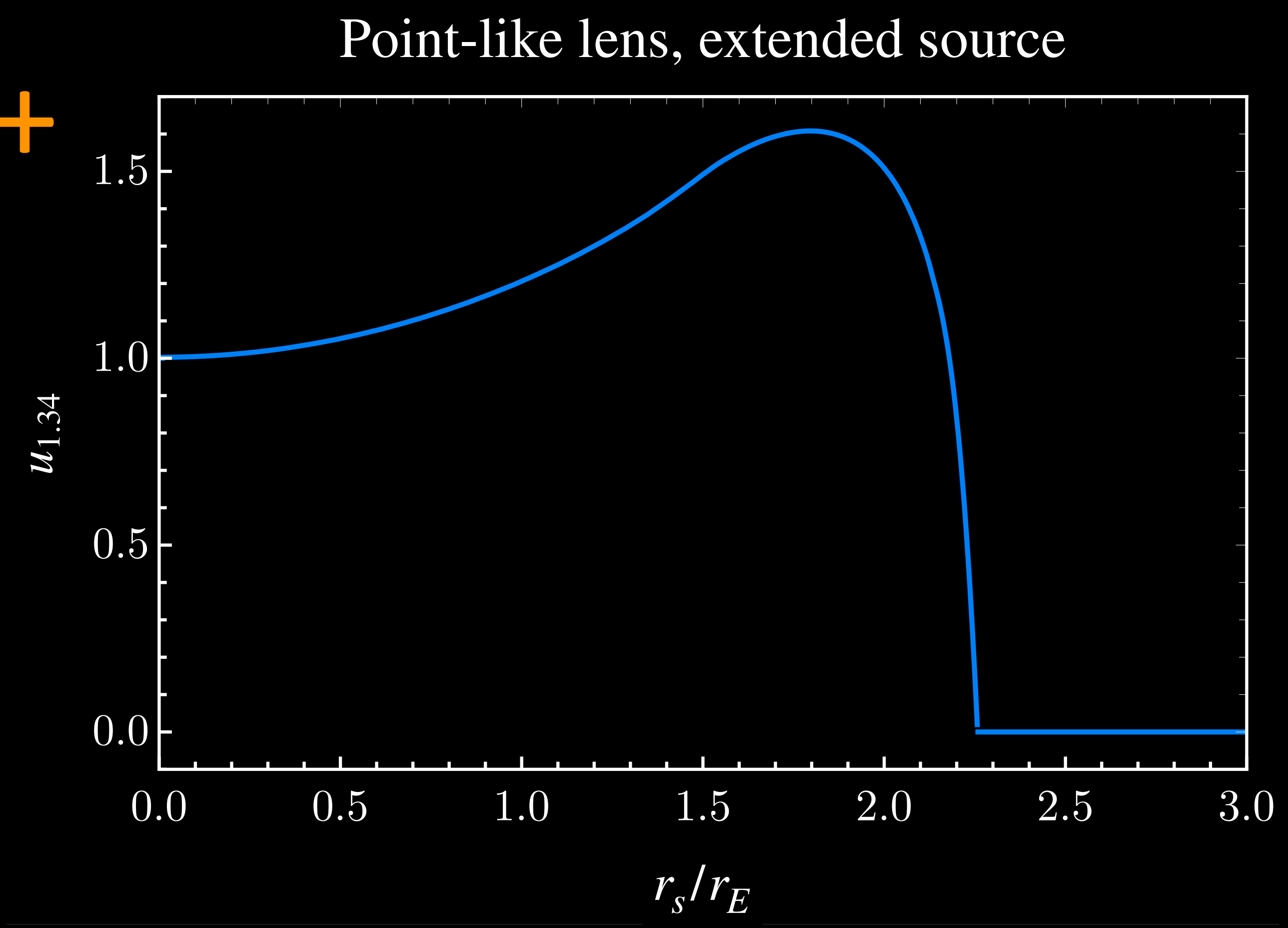

For point-like lenses, see for example,
Witt and Mao, Astrophys. J (1994);
Montero-Camacho, Fang, Vasquez, Silva, Hirata, [JCAP, arXiv:1906.05950];
Smyth, Profumo, English, Jeltema, McKinnon, Guhathakurta [PRD, arXiv:1910.01285];

Extended sources: $r_E = \theta_E D_L \sim r_S$

Same procedure as before, but now $u_{1.34}$ is a function of both r_{90} and r_S

DC, D. McKeen, N. Raj, Z. Wang, PRD, arXiv:2007.12697 [astro-ph.CO]

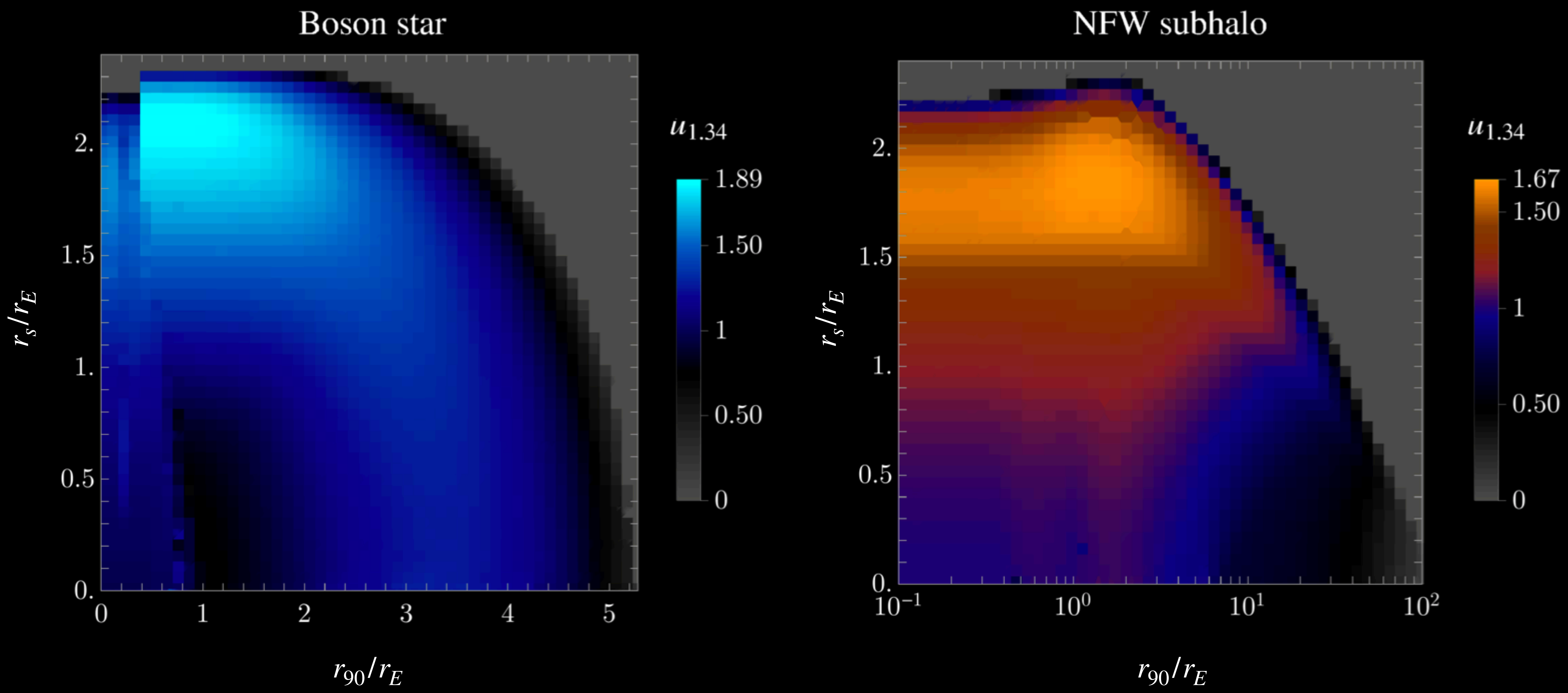

DC, D. McKeen, N. Raj, Z. Wang, PRD, arXiv:2007.12697 [astro-ph.CO]

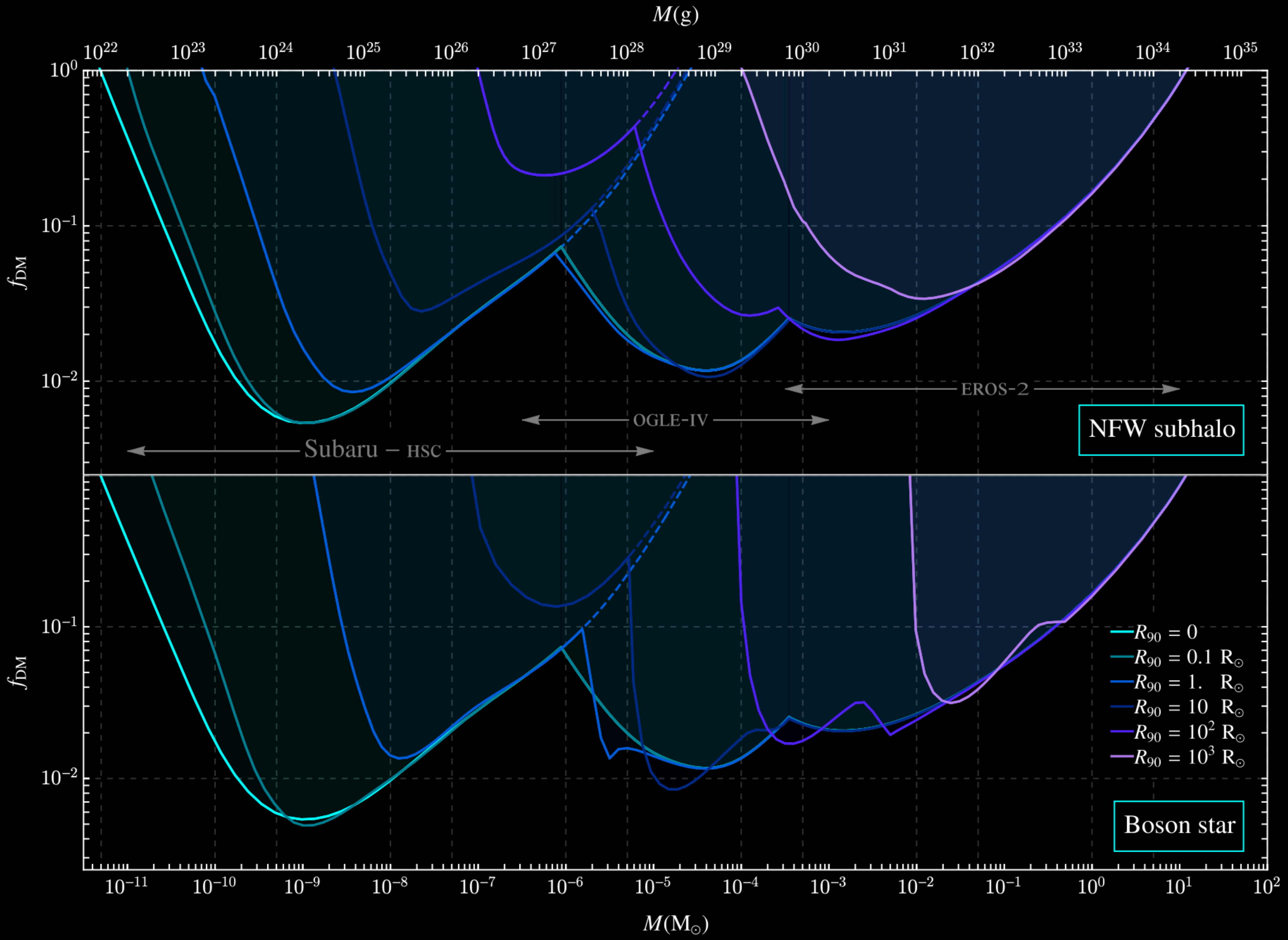

DC, Sevillano Muñoz arXiv:2403.13072

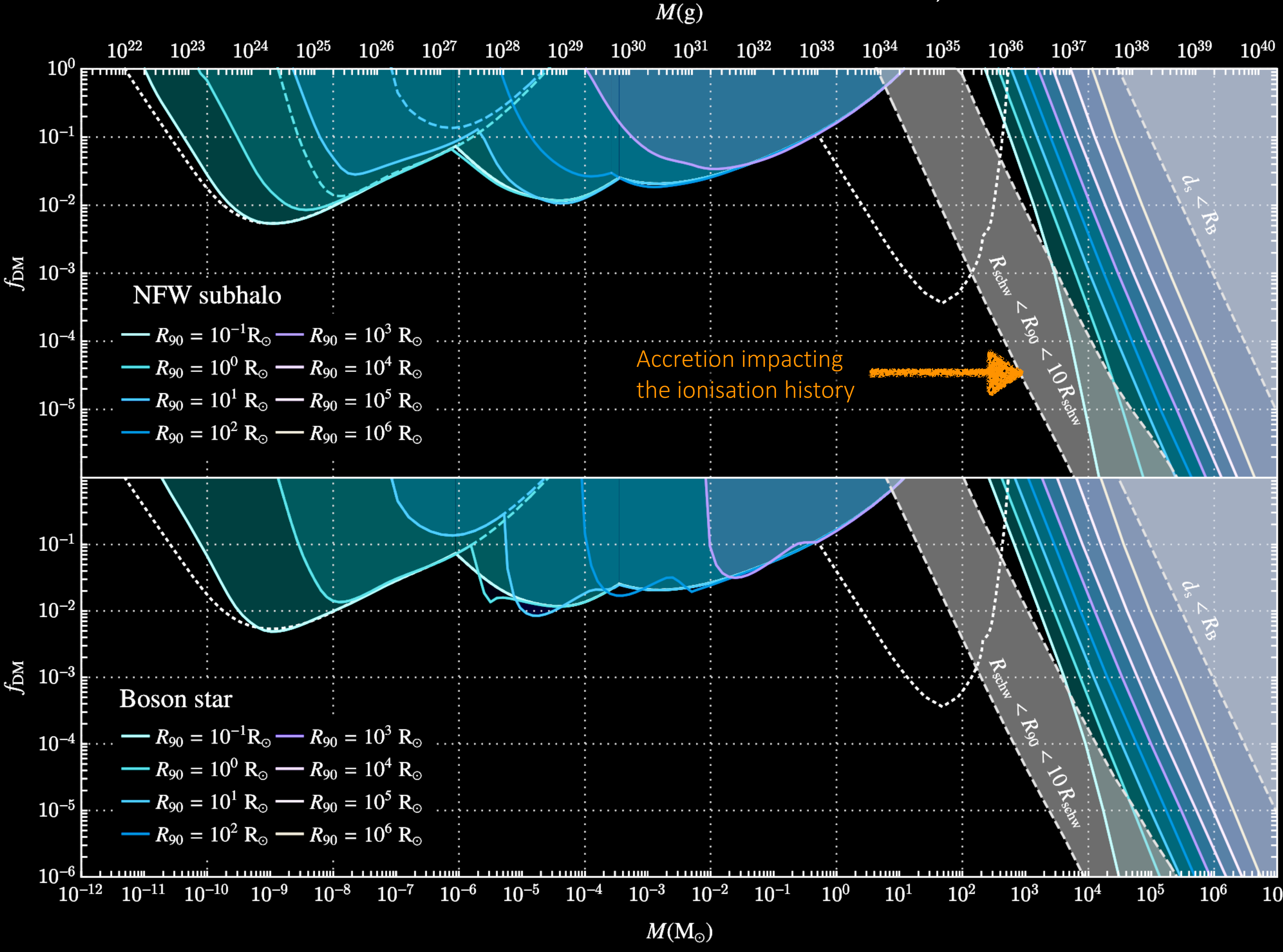

Accretion impacting the ionisation history

BS light curves have different shapes

Miguel Crispim-Romao, DC, arXiv:2402.00107

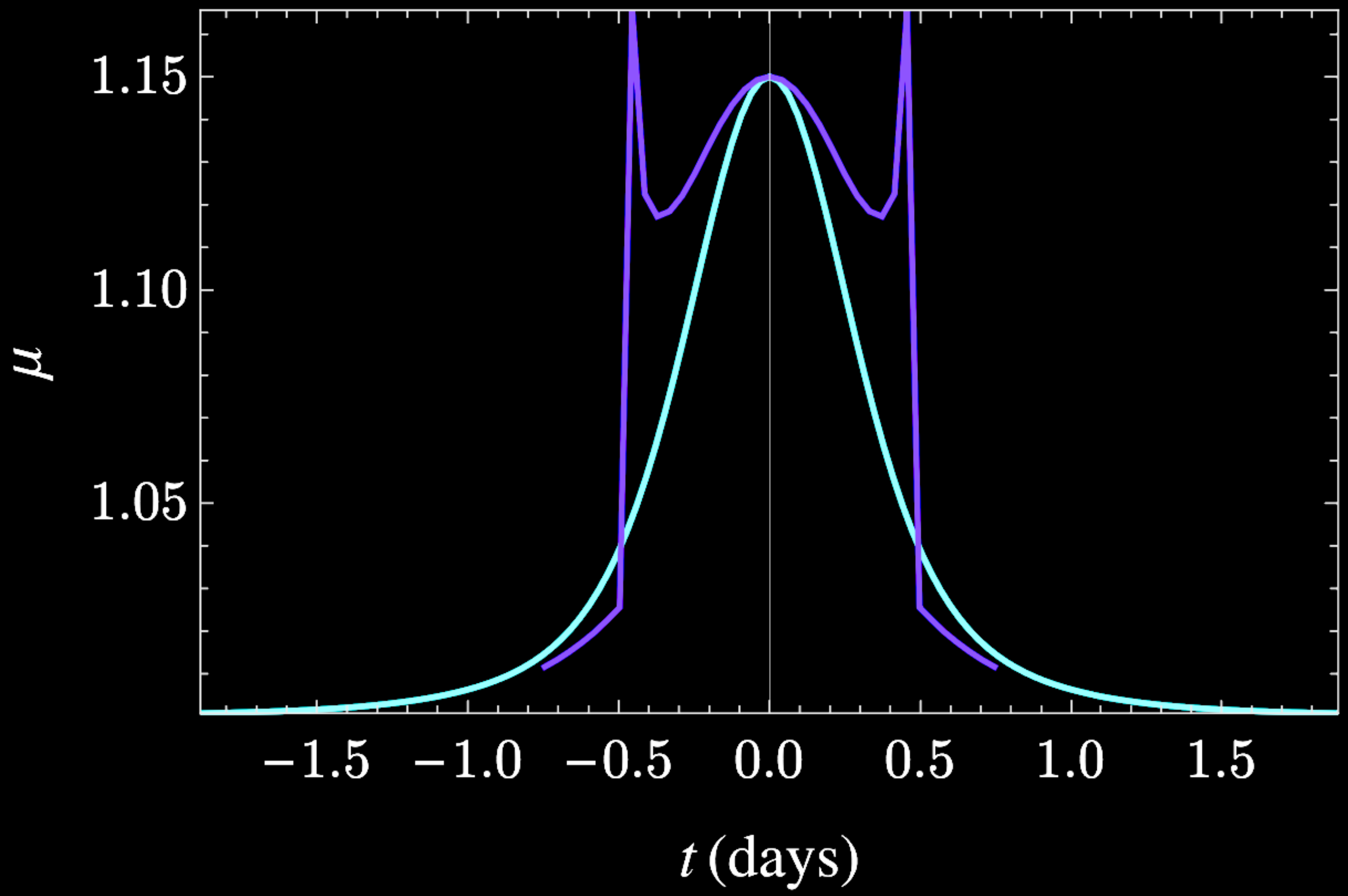

$\tau = \theta/\theta_E$

$\tau_m \equiv \theta_{\text{lens}}/\theta_E = r_{\text{lens}}/r_E$

Boson star with $\tau_m = 1$

PBH (or $\tau_m = 0$)

BS light curves have different shapes

Miguel Crispim-Romao, DC, arXiv:2402.00107

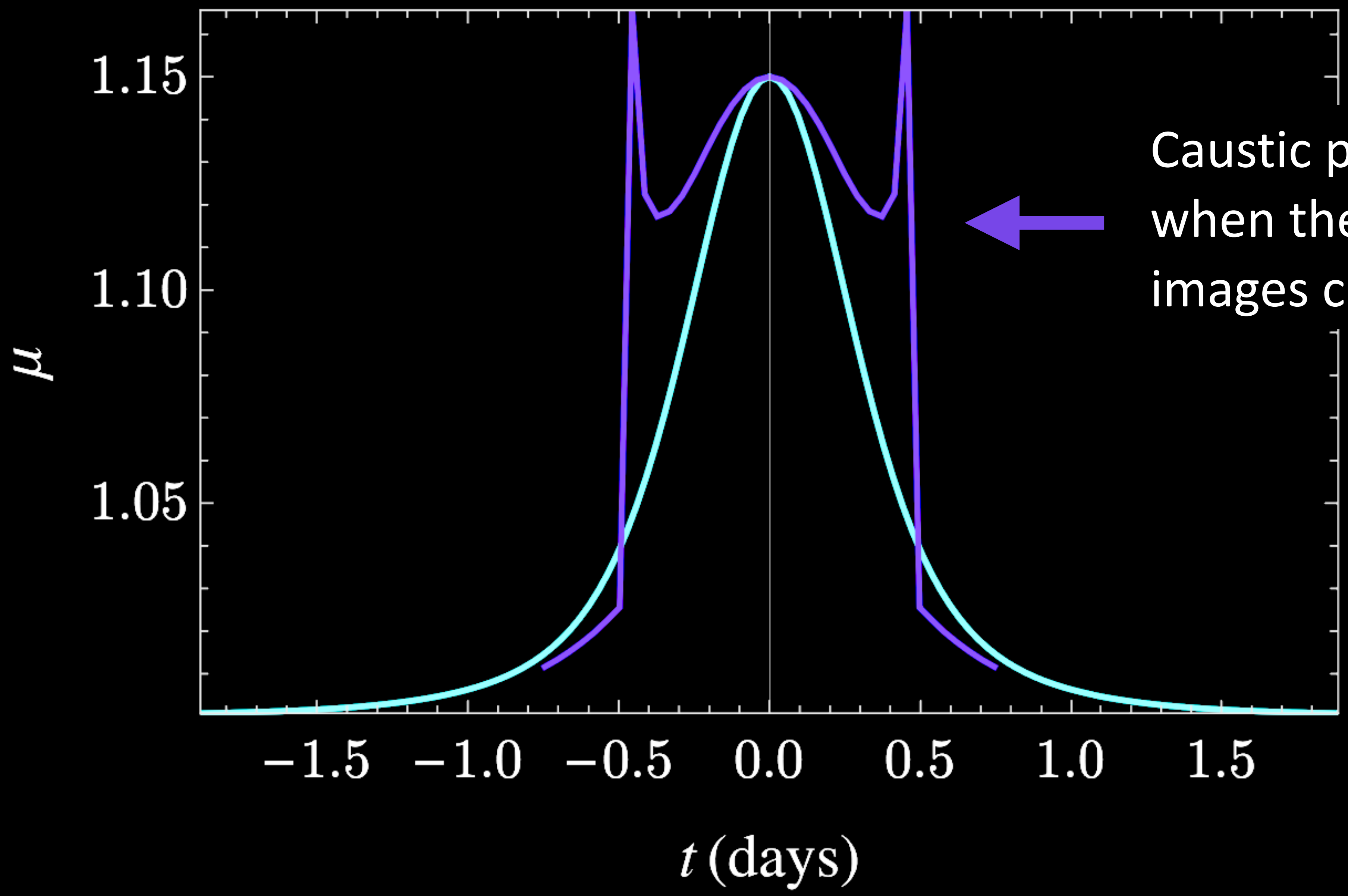

Caustic peaks can arise when the number of images changes

Boson star with $\tau_m = 1$

PBH (or $\tau_m = 0$)

BS light curves have different shapes

Miguel Crispim-Romao, DC, arXiv:2402.00107

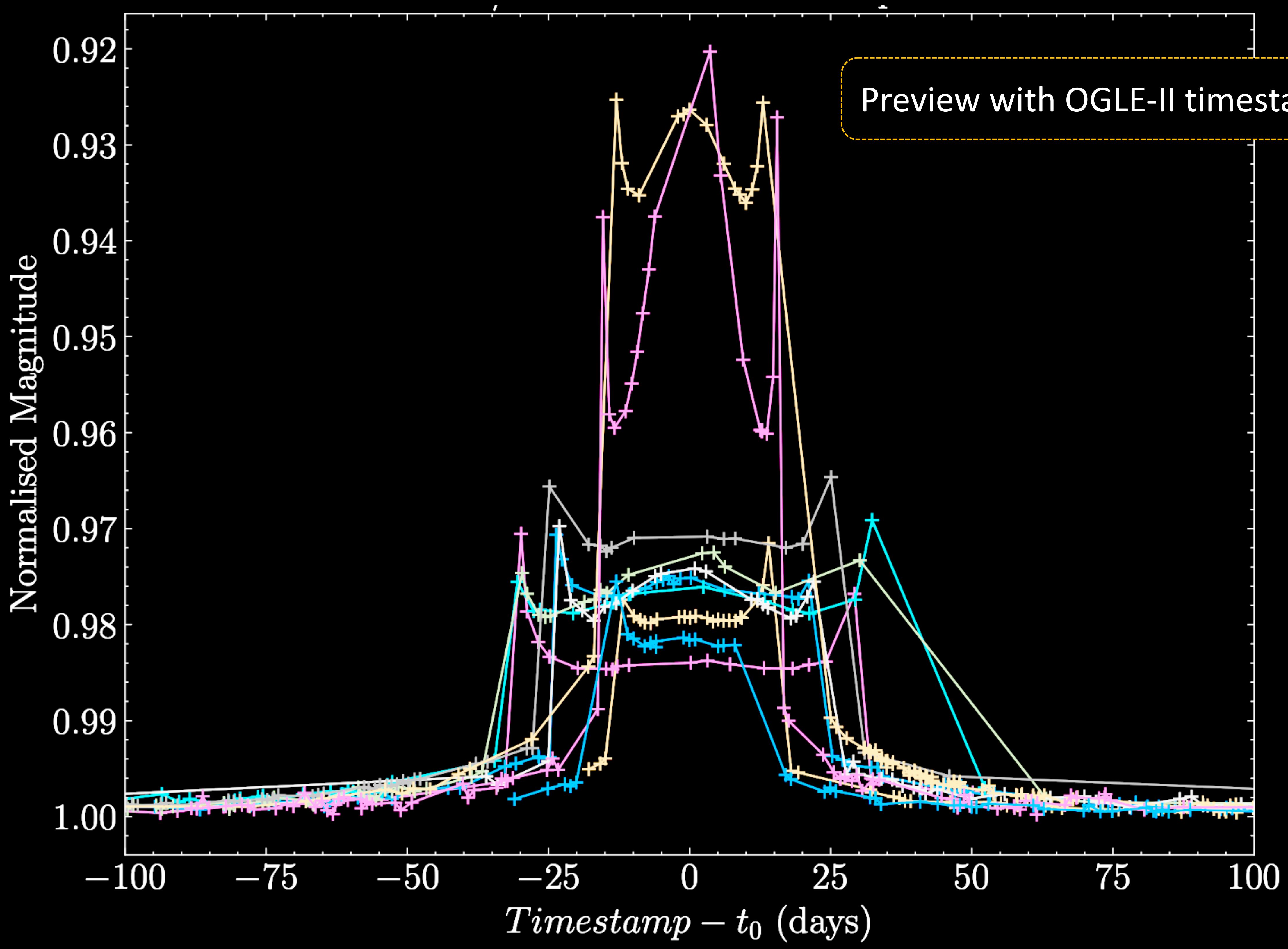

Preview with OGLE-II timestamps

Miguel Crispim-Romao, DC, arXiv:2402.00107

ML + ML

Microlensing + Machine Learning

- Microlensing data is time series data
- Challenge: low-cadence data, lower signal-to-noise ratios

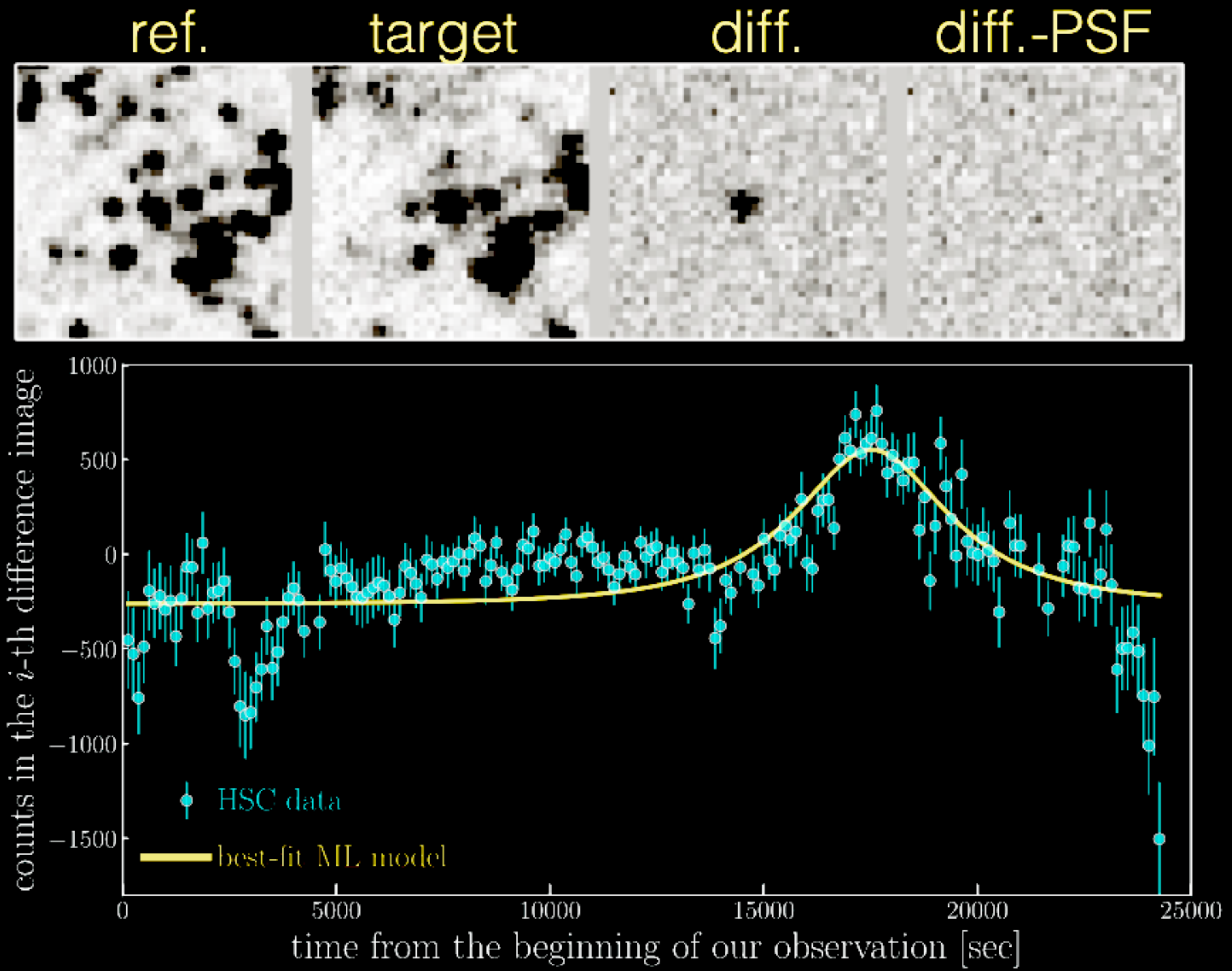

From the Subaru collaboration, arXiv:1701.02151

Miguel Crispim-Romao, DC, arXiv:2402.00107

ML + ML

Microlensing + Machine Learning

- Microlensing data is time series data
- Challenge: low-cadence data, lower signal-to-noise ratios
- MicroLIA: use a Random Forest (RF) algorithm to find microlensing event (and distinguish from other events)

Godines et al, arXiv:2004.14347

Miguel Crispim-Romao, DC, arXiv:2402.00107

ML + ML

Microlensing + Machine Learning

- Microlensing data is time series data
- Challenge: low-cadence data, lower signal-to-noise ratios
- MicroLIA: use a Random Forest (RF) algorithm to find microlensing event (and distinguish from other events)

Our adaptations:

- Implement boson star and NFW light curves with $0.5 < \tau_m < 5$
- Instead of an RF, we use a histogram-based gradient boosted classifier (HBGC) to improve speed
- Add criterium $\mu \geq 1.34$

(… and a few fixes)

Complete datasets not available

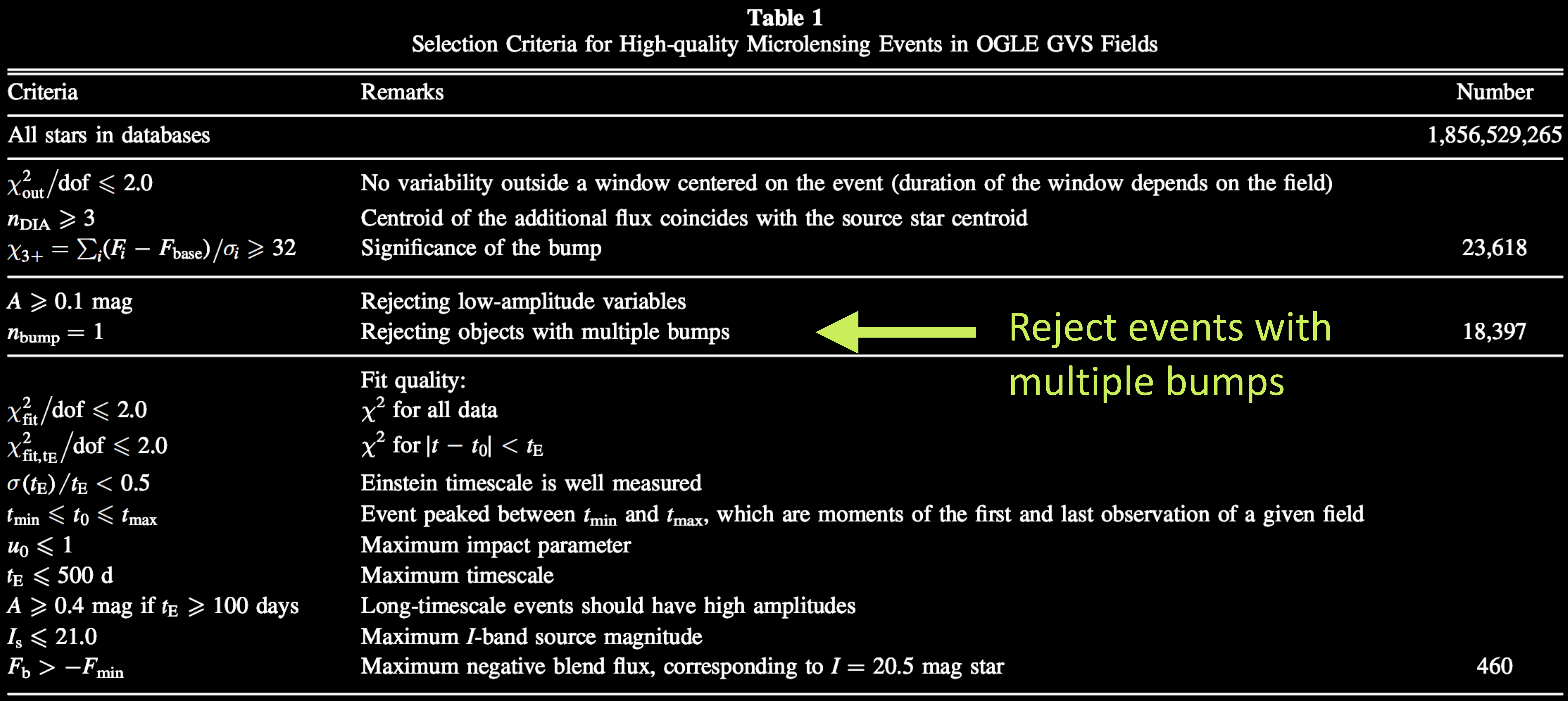

Table 1
Selection Criteria for High-quality Microlensing Events in OGLE GVS Fields

Criteria	Remarks	Number
All stars in databases		1,856,529,265
$\chi^2_{\rm out}/{\rm dof} \leqslant 2.0$	No variability outside a window centered on the event (duration of the window depends on the field)	
$n_{\rm DIA} \geqslant 3$	Centroid of the additional flux coincides with the source star centroid	
$\chi_{3+} = \sum_i (F_i - F_{\rm base})/\sigma_i \geqslant 32$	Significance of the bump	23,618
$A \geqslant 0.1$ mag	Rejecting low-amplitude variables	
$n_{\rm bump} = 1$	Rejecting objects with multiple bumps	18,397
	Fit quality:	
$\chi^2_{\rm fit}/{\rm dof} \leqslant 2.0$	χ^2 for all data	
$\chi^2_{\rm fit,tE}/{\rm dof} \leqslant 2.0$	χ^2 for $\lvert t - t_0 \rvert < t_{\rm E}$	
$\sigma(t_{\rm E})/t_{\rm E} < 0.5$	Einstein timescale is well measured	
$t_{\rm min} \leqslant t_0 \leqslant t_{\rm max}$	Event peaked between $t_{\rm min}$ and $t_{\rm max}$, which are moments of the first and last observation of a given field	
$u_0 \leqslant 1$	Maximum impact parameter	
$t_{\rm E} \leqslant 500$ d	Maximum timescale	
$A \geqslant 0.4$ mag if $t_{\rm E} \geqslant 100$ days	Long-timescale events should have high amplitudes	
$I_{\rm s} \leqslant 21.0$	Maximum I-band source magnitude	
$F_{\rm b} > -F_{\rm min}$	Maximum negative blend flux, corresponding to $I = 20.5$ mag star	460

Reject events with multiple bumps

So for now… generating and injecting events

-

Confusion Matrix All vs All
w/ OGLE-II Timestamps

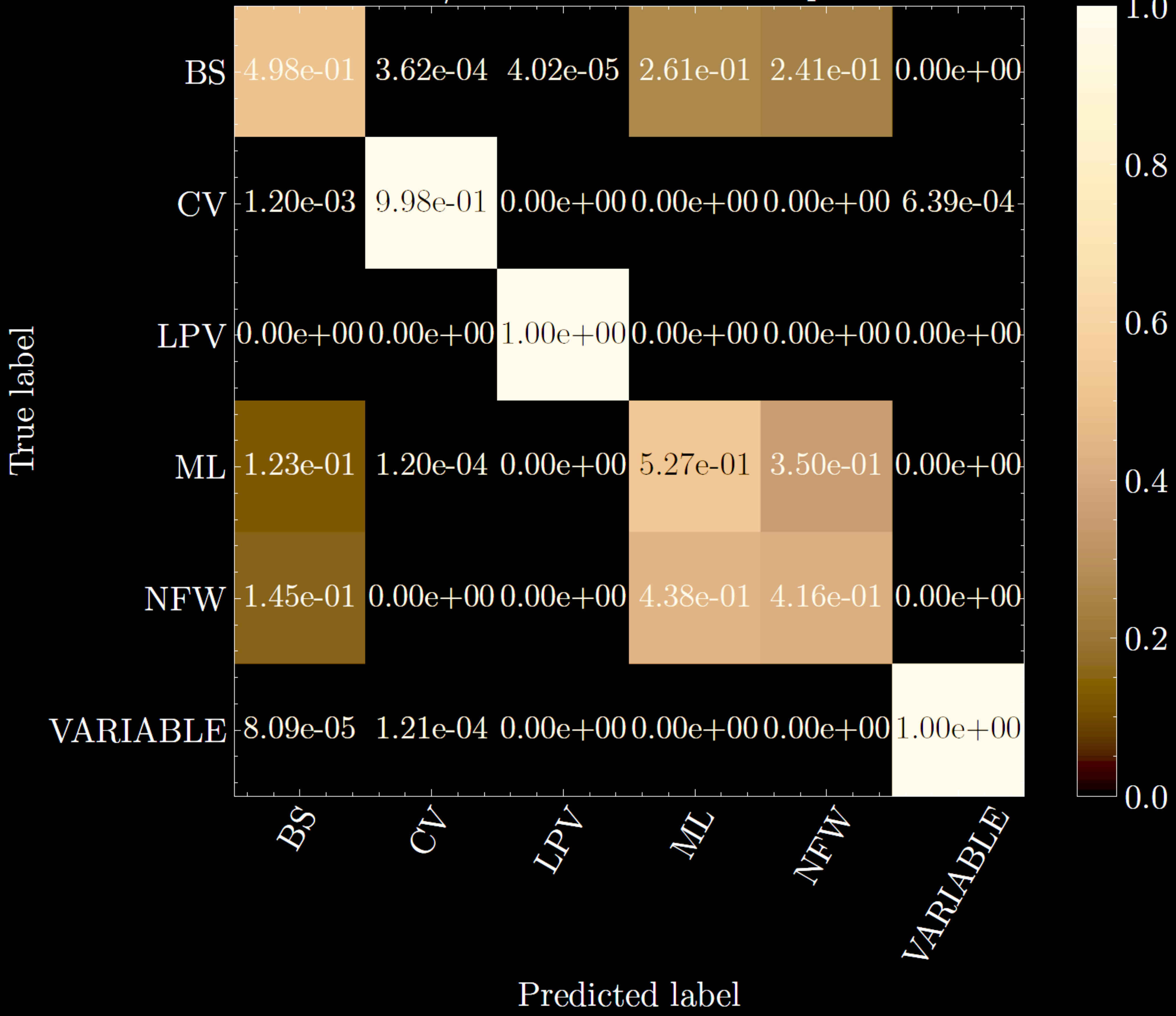

True label \ Predicted label	BS	CV	LPV	ML	NFW	VARIABLE
BS	4.98e-01	3.62e-04	4.02e-05	2.61e-01	2.41e-01	0.00e+00
CV	1.20e-03	9.98e-01	0.00e+00	0.00e+00	0.00e+00	6.39e-04
LPV	0.00e+00	0.00e+00	1.00e+00	0.00e+00	0.00e+00	0.00e+00
ML	1.23e-01	1.20e-04	0.00e+00	5.27e-01	3.50e-01	0.00e+00
NFW	1.45e-01	0.00e+00	0.00e+00	4.38e-01	4.16e-01	0.00e+00
VARIABLE	8.09e-05	1.21e-04	0.00e+00	0.00e+00	0.00e+00	1.00e+00

Miguel Crispim-Romao, DC, arXiv:2402.00107

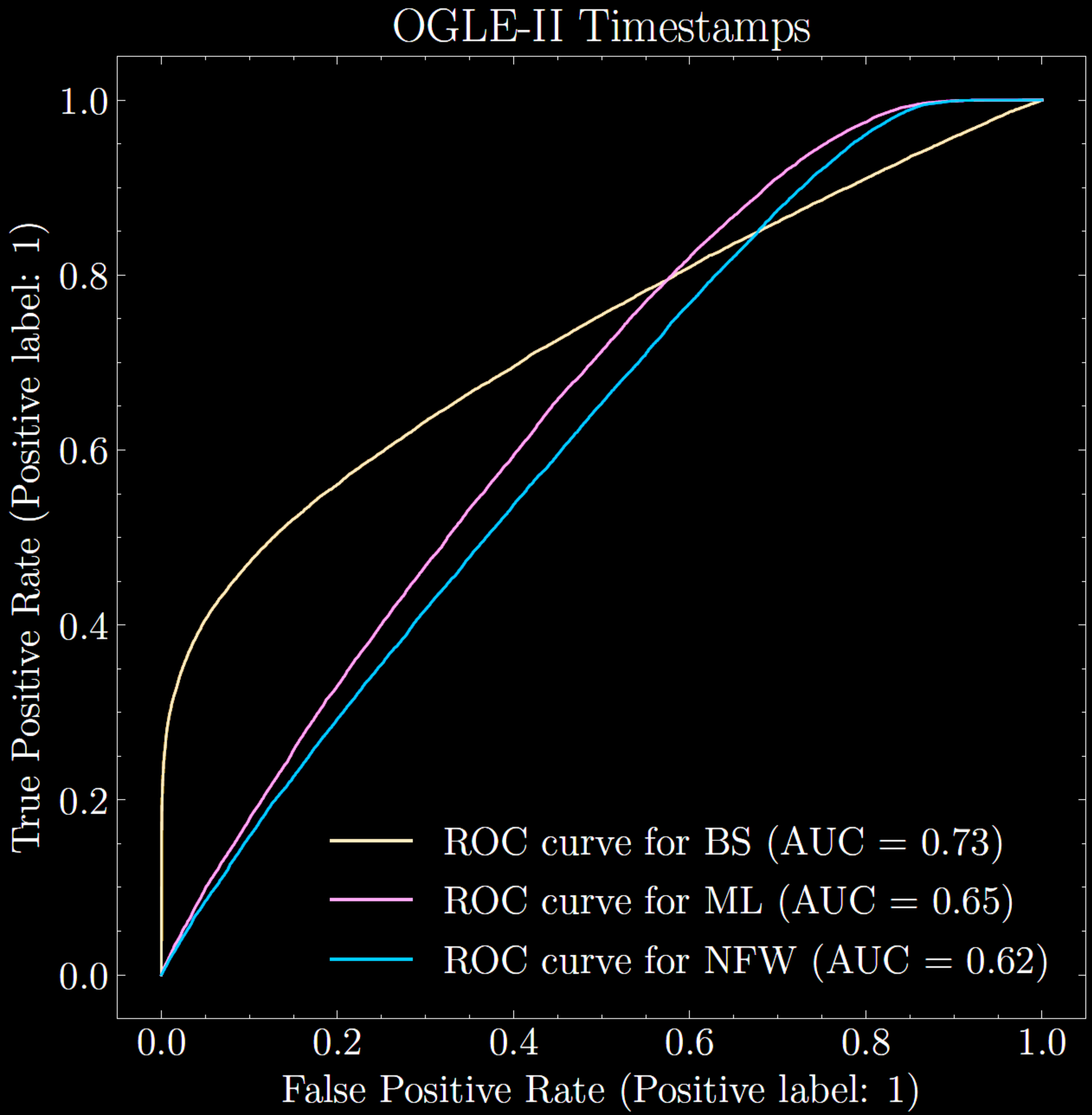

Miguel Crispim-Romao, DC, arXiv:2402.00107

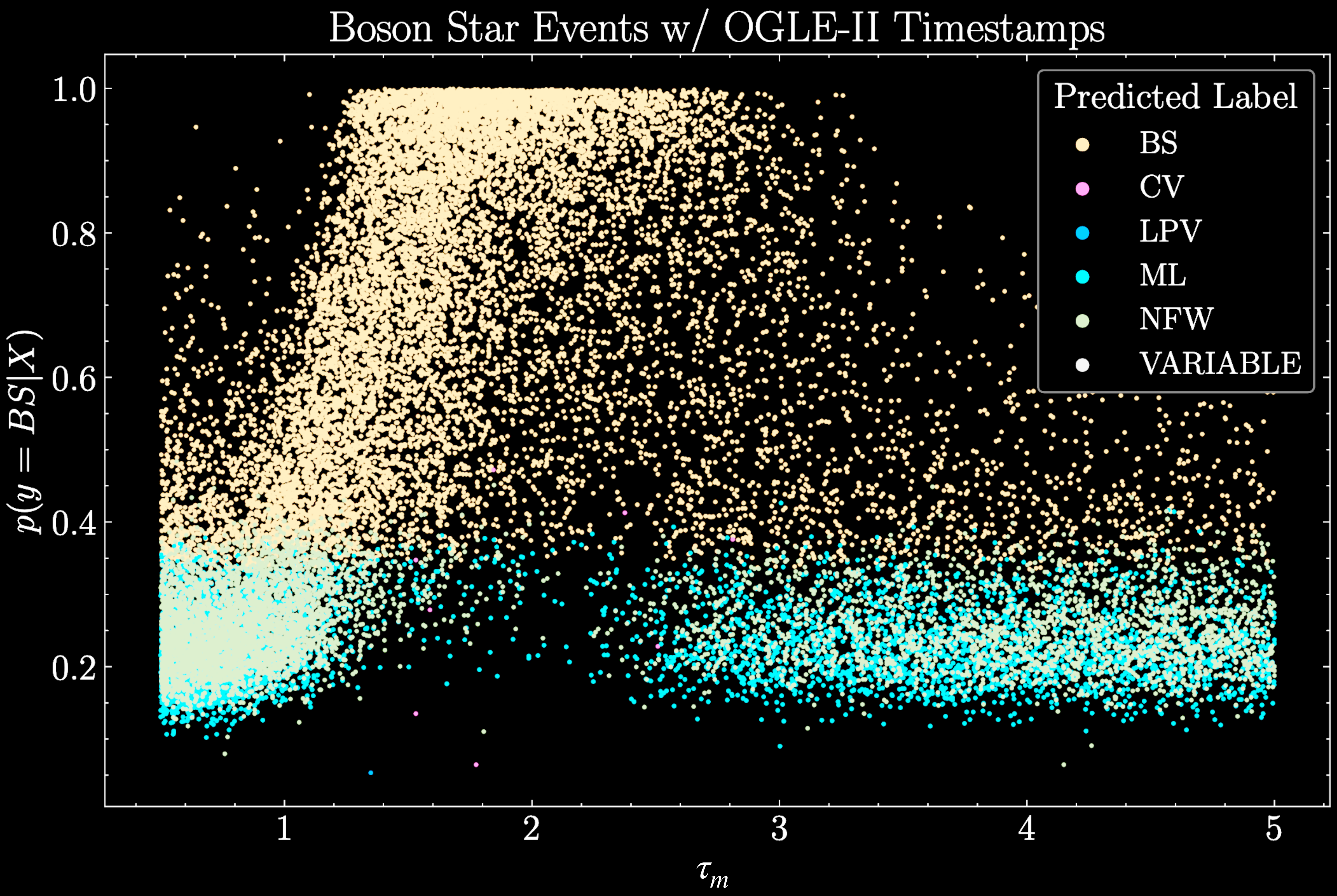

Miguel Crispim-Romao, DC, arXiv:2402.00107

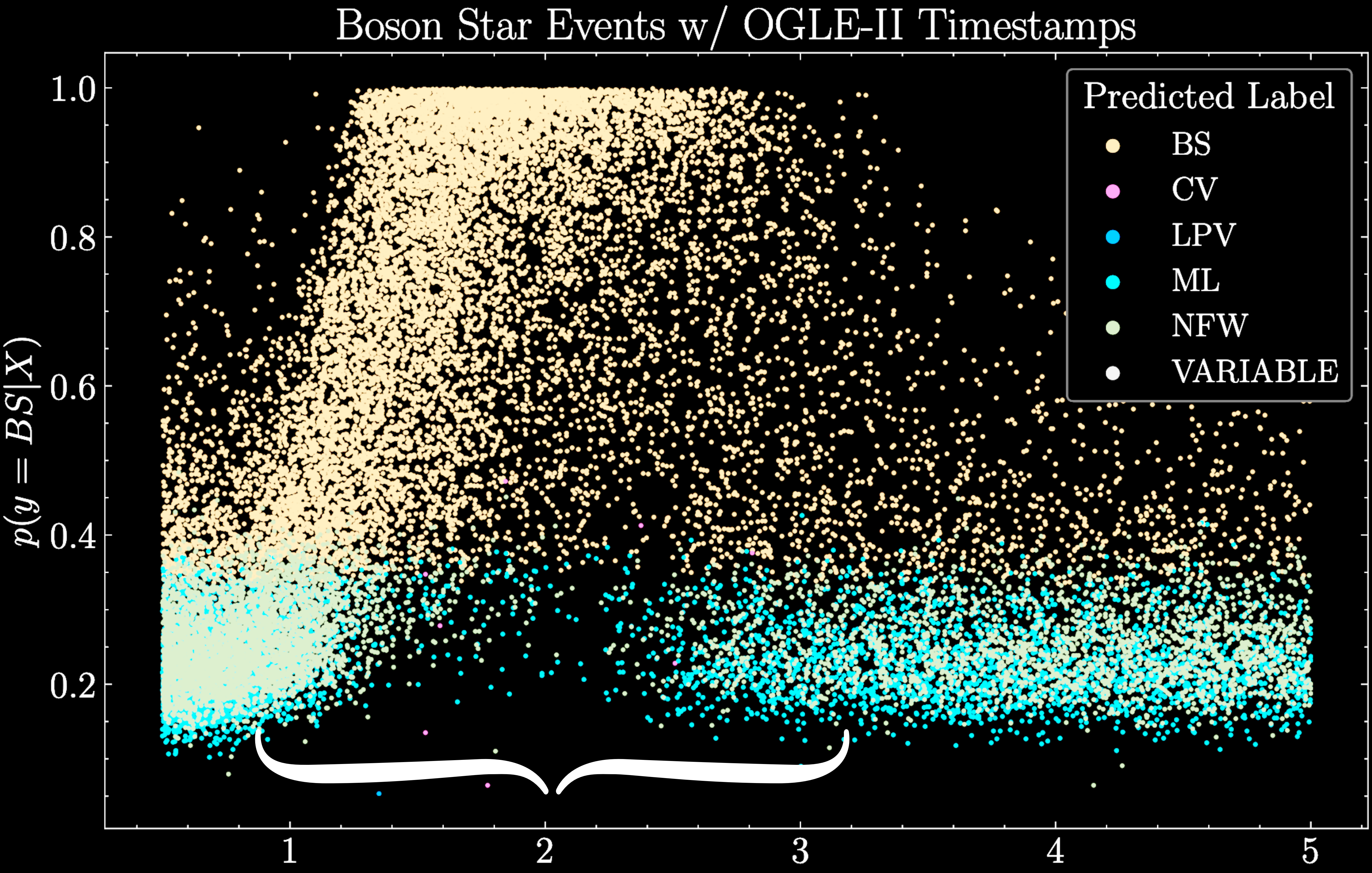

Indeed, the most probable detections are for $0.8 < \tau_m < 3$

Now, let’s dream…

- The OGLE time steps are quite irregular
- Many different factors play a role…
  - Observational Constraints (weather, moon phase, …)
  - Resource Allocation
  - Target Prioritization
  - Technical Maintenance and Downtime

- But it is interesting what the effect of cadence (ir)regularity is on the observational prospects
- So, let us imagine for a moment that we could achieve perfect daily cadence

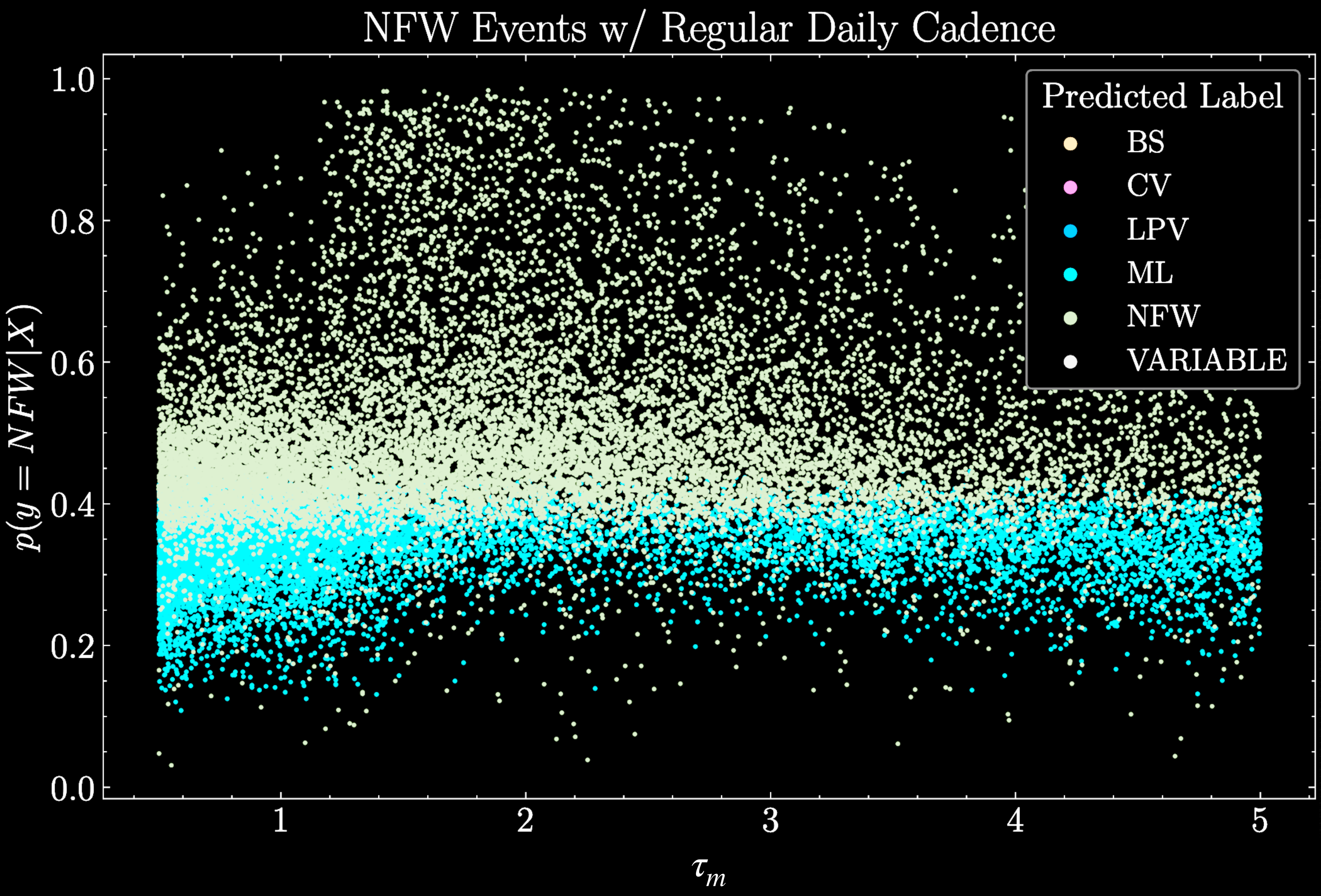

Miguel Crispim-Romao, DC, arXiv:2402.00107

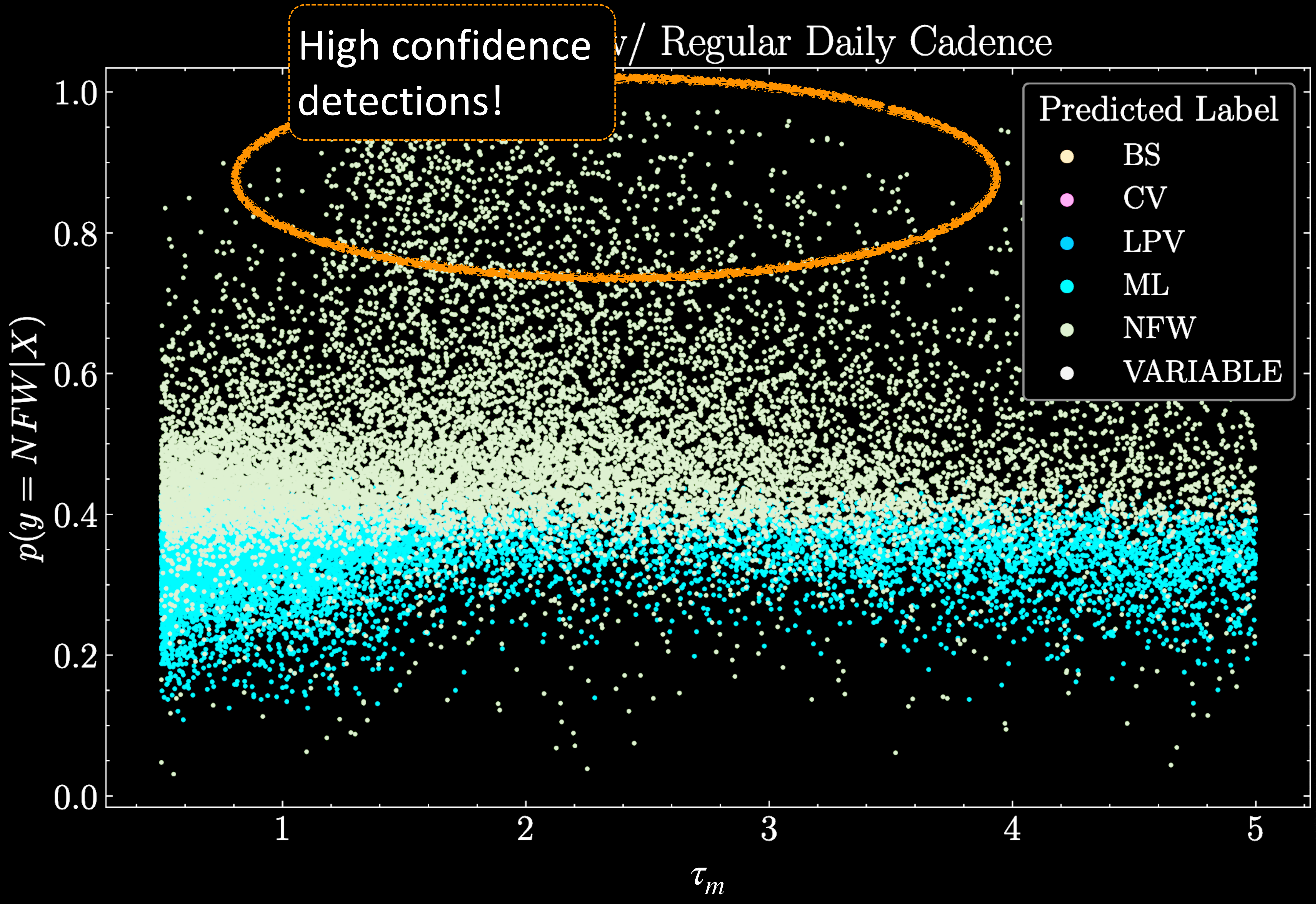

High confidence detections!

… only observed if regular cadence is achieved

Miguel Crispim-Romao, DC, arXiv:2402.00107

Current work

Teamed up with MicroLIA's main author Daniel Godines (and Miguel)

- ELAsTiCC dataset (Extended LSST Astronomical Time Series Classification Challenge)
  - Multiple sources, galactic and extragalactic
  - Science purposed

ELAsTiCC presents the first simulation of LSST alerts, with millions of synthetic transient light curves and host galaxies. The data is being used to test broker alert systems and classifiers, and develop the infrastructure for LSST's Dark Energy Science Collaboration Time-Domain needs.

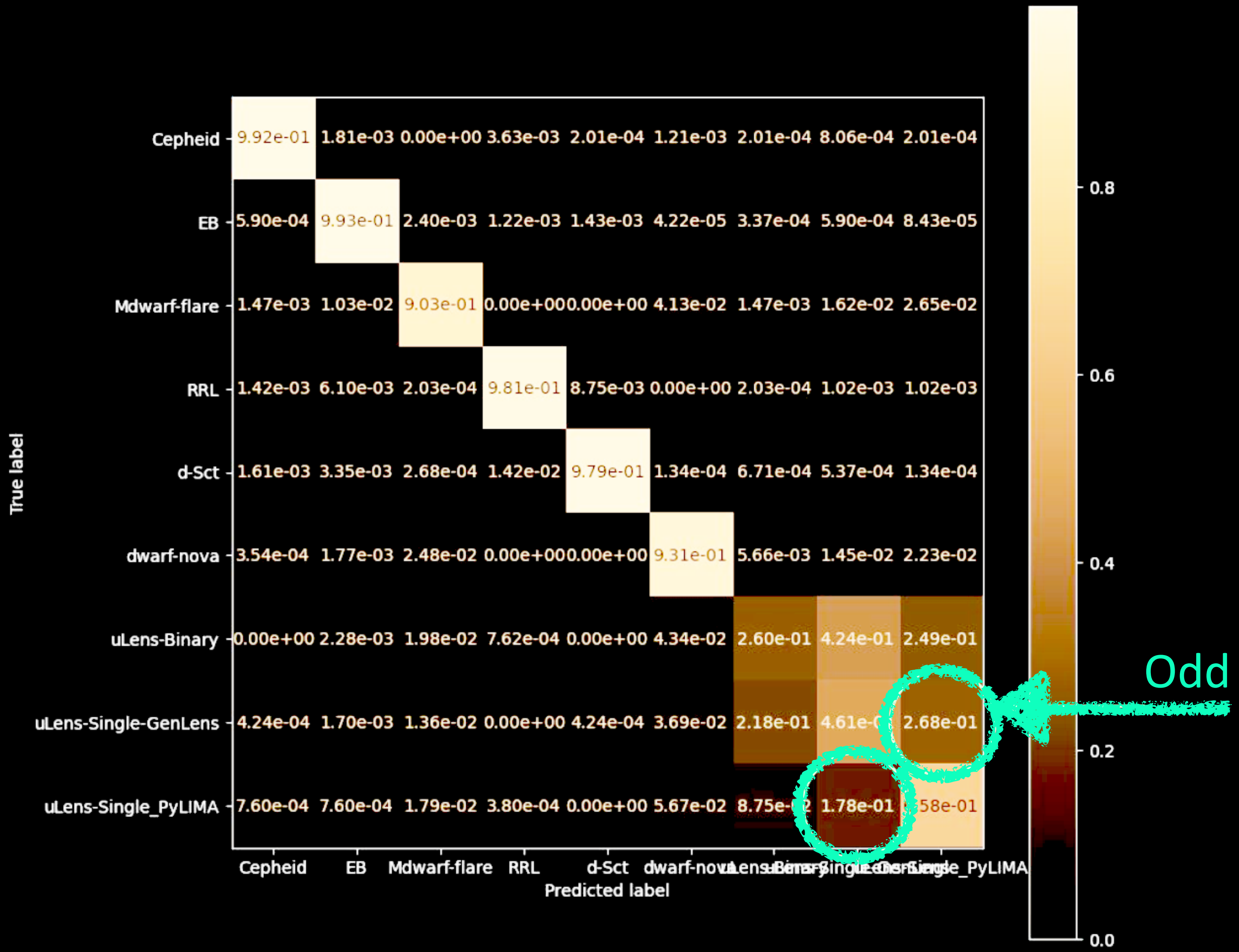

	Cepheid	EB	Mdwarf-flare	RRL	d-Sct	dwarf-nova	uLens-Binary	uLens-Single-GenLens	uLens-Single_PyLIMA
Cepheid	9.92e-01	1.81e-03	0.00e+00	3.63e-03	2.01e-04	1.21e-03	2.01e-04	8.06e-04	2.01e-04
EB	5.90e-04	9.93e-01	2.40e-03	1.22e-03	1.43e-03	4.22e-05	3.37e-04	5.90e-04	8.43e-05
Mdwarf-flare	1.47e-03	1.03e-02	9.03e-01	0.00e+00	0.00e+00	4.13e-02	1.47e-03	1.62e-02	2.65e-02
RRL	1.42e-03	6.10e-03	2.03e-04	9.81e-01	8.75e-03	0.00e+00	2.03e-04	1.02e-03	1.02e-03
d-Sct	1.61e-03	3.35e-03	2.68e-04	1.42e-02	9.79e-01	1.34e-04	6.71e-04	5.37e-04	1.34e-04
dwarf-nova	3.54e-04	1.77e-03	2.48e-02	0.00e+00	0.00e+00	9.31e-01	5.66e-03	1.45e-02	2.23e-02
uLens-Binary	0.00e+00	2.28e-03	1.98e-02	7.62e-04	0.00e+00	4.34e-02	2.60e-01	4.24e-01	2.49e-01
uLens-Single-GenLens	4.24e-04	1.70e-03	1.36e-02	0.00e+00	4.24e-04	3.69e-02	2.18e-01	4.61e-[illegible]	2.68e-01
uLens-Single_PyLIMA	7.60e-04	7.60e-04	1.79e-02	3.80e-04	0.00e+00	5.67e-02	8.75e-[illegible]2	1.78e-01	[illegible]58e-01

To conclude,

- All of our current evidence for Dark Matter is gravitational; many dark matter models feature substructure

- Microlensing provides a way to look for dark matter substructure of a large range of sizes and masses
  - → Extended objects may give unique microlensing signatures
  - → Non-observation can be used to derive constraints

- Microlensing signatures of extended objects can be distinguished using machine learning

- Future work: comparing to all events in ELaSTiCC, deep learning on the light curves, …

Thank you!

…ask me anything you like!

djuna.l.croon@durham.ac.uk | djunacroon.com

Back up slides

Case study 1: NFW-halo mass profile

- Well-known halo profile: $\rho(r) = \dfrac{\rho_\mathrm{s}}{(r/r_\mathrm{s})(1 + r/r_\mathrm{s})^2}$

- As the mass inclosed formally diverges, we cut it off at $R_\mathrm{cut} = 100\, R_\mathrm{sc}$
- Enclosed mass $\propto \log(\kappa + 1) - (\kappa/(\kappa + 1))$ where $\kappa = R_\mathrm{cut}/R_\mathrm{sc}$

- Computing $m(\tau)$ is then a trivial exercise:

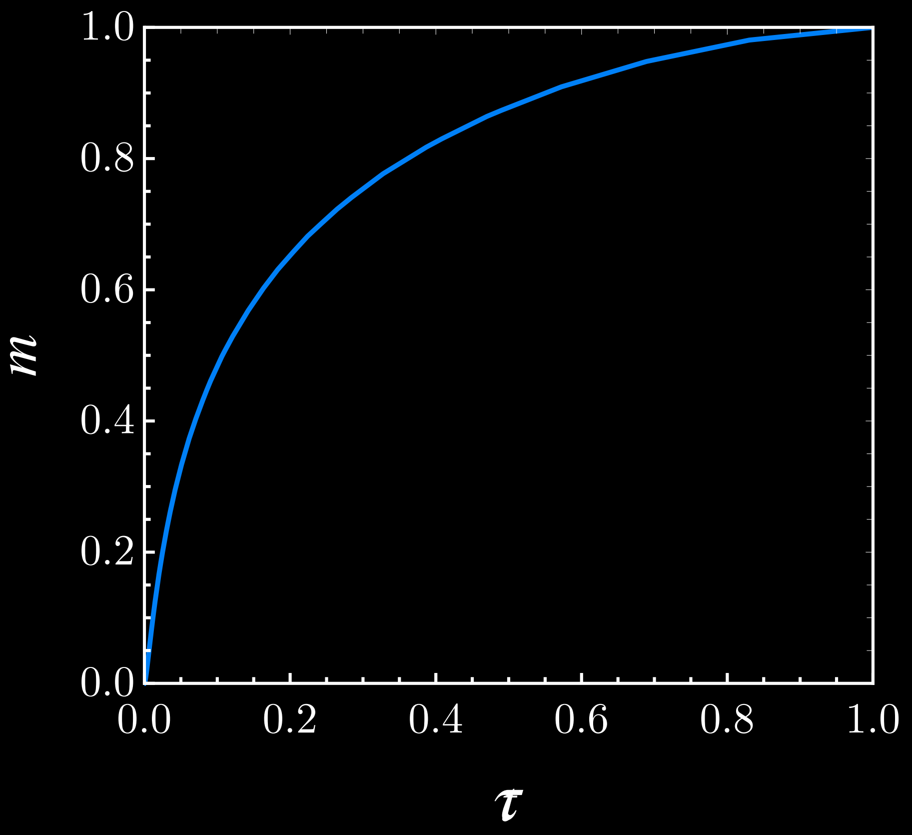

Case study 2: Boson star mass profile

- The Schrodinger-Poisson equation,

$$\mu\Psi = -\frac{1}{2m_\phi}\left(\Psi'' + \frac{2}{r}\Psi'\right) + m_\phi \Phi\Psi$$

Describes the radial distribution

describes a *spherically symmetric ground state of a free scalar field in the non-relativistic limit*

- The mass enclosed is given by

$$M_{\rm BS}(r) = \frac{1}{m_\phi G}\int_0^{m_\phi r} dy\ y^2\ \Psi^2(y)$$

from which $m(\tau)$ may be computed

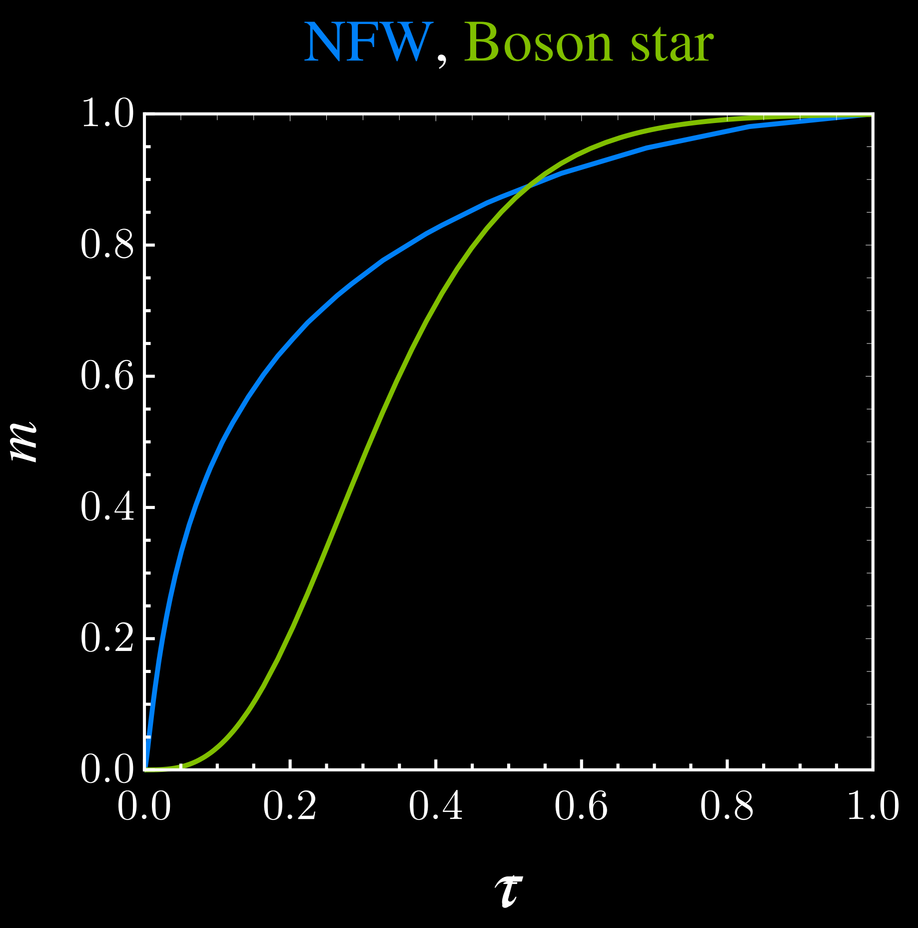

Caustics

What's going on in this plot?

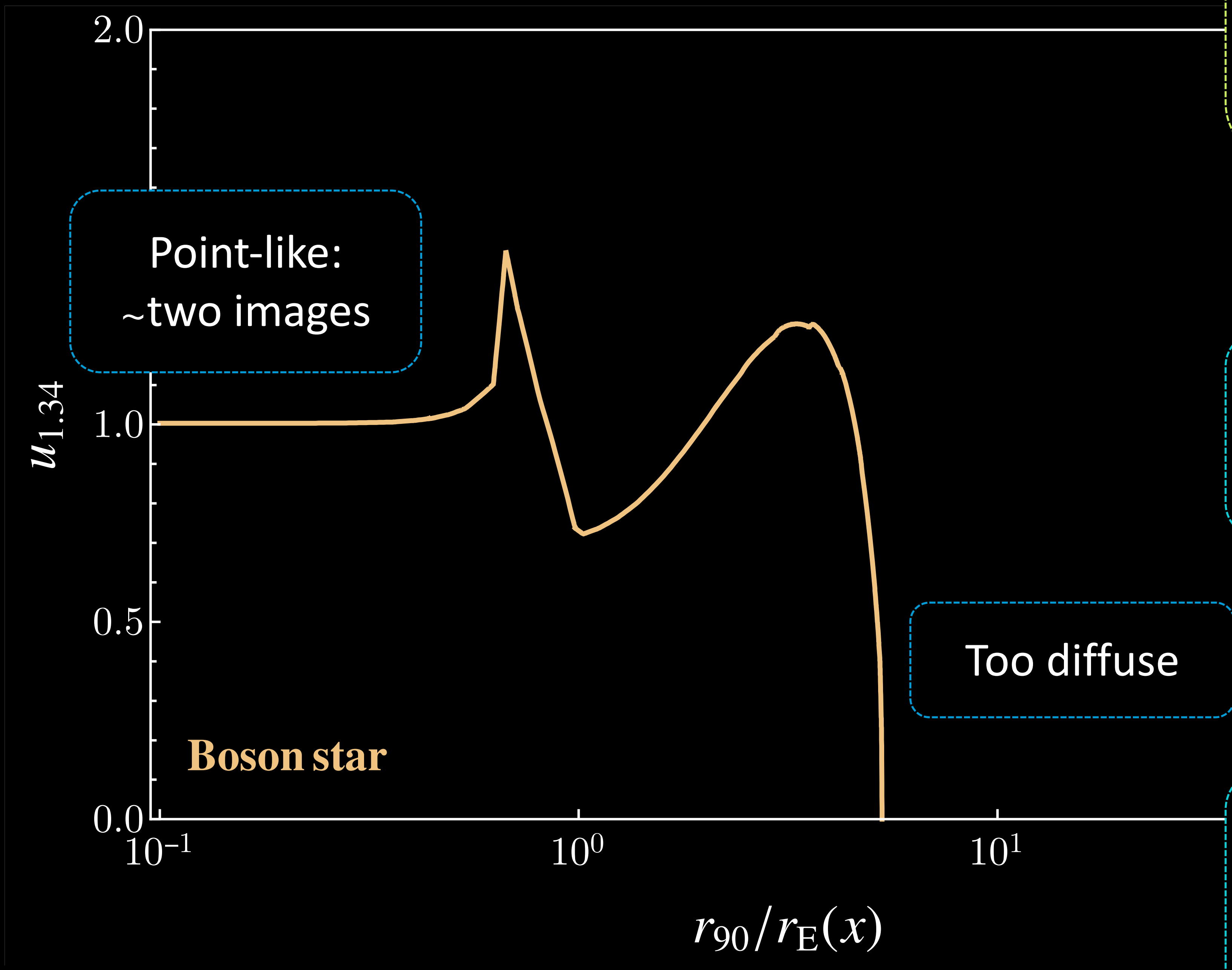

Point-like:
~two images

Too diffuse

Sufficiently flat density profiles can give more or fewer lens images (solutions to the lens equation) compared to a point-like lens

→ Objects such as boson stars may give unique microlensing signals

→ Constraints on the dark matter subfraction may be stronger or weaker than for point-like lenses

Caustics

What's going on in this plot?

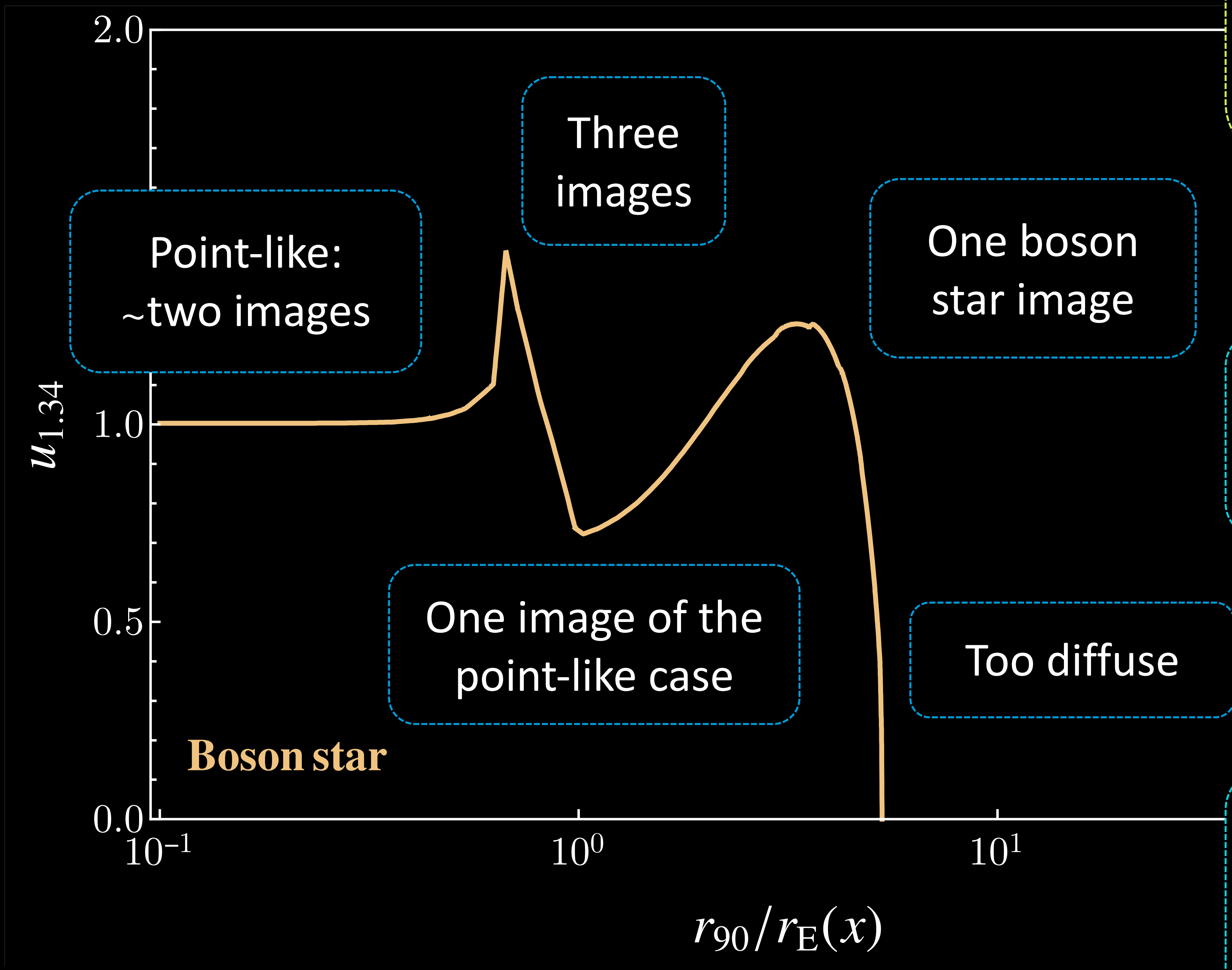

Sufficiently flat density profiles can give more or fewer lens images (solutions to the lens equation) compared to a point-like lens

→ Objects such as boson stars may give unique microlensing signals

→ Constraints on the dark matter subfraction may be stronger or weaker than for point-like lenses

Caustics

Consequence: the Einstein tube is not a tube; not ellipsoidal

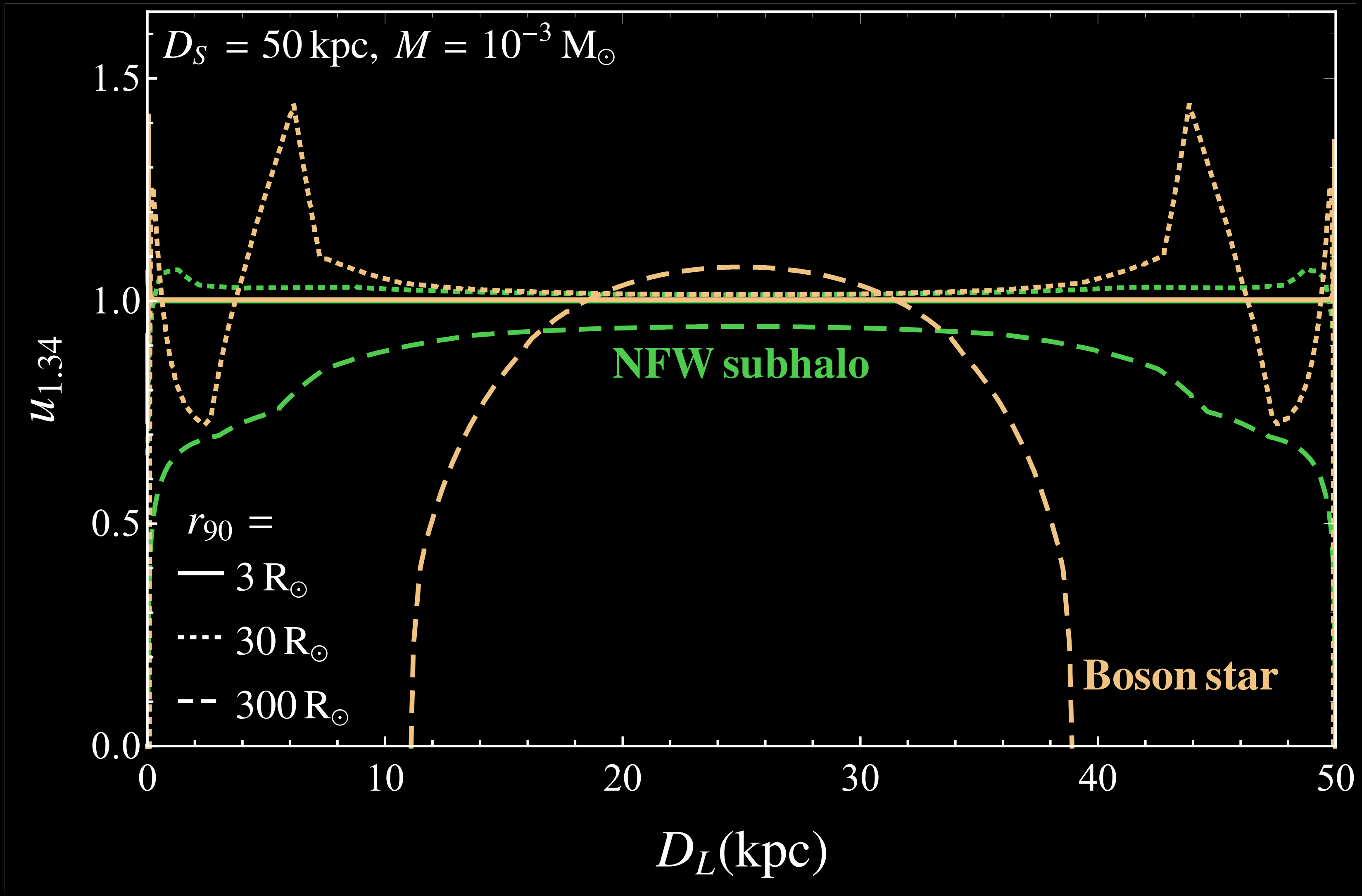

→ Depending on the source, experiments may be more or less sensitive to extended objects compared to point sources in different locations

Constraining extended objects

The differential event rate contains all the essential physics

$$x = \frac{D_\mathrm{L}}{D_\mathrm{S}}$$

$$\frac{d^2\Gamma}{dx\,dt_\mathrm{E}} = \varepsilon(t_\mathrm{E})\frac{2D_\mathrm{S}}{v_0^2 M} f_\mathrm{DM}\rho_\mathrm{DM}(x)v_\mathrm{E}^4(x)e^{-v_\mathrm{E}^2(x)/v_0^2}$$

Constraining extended objects

The differential event rate contains all the essential physics

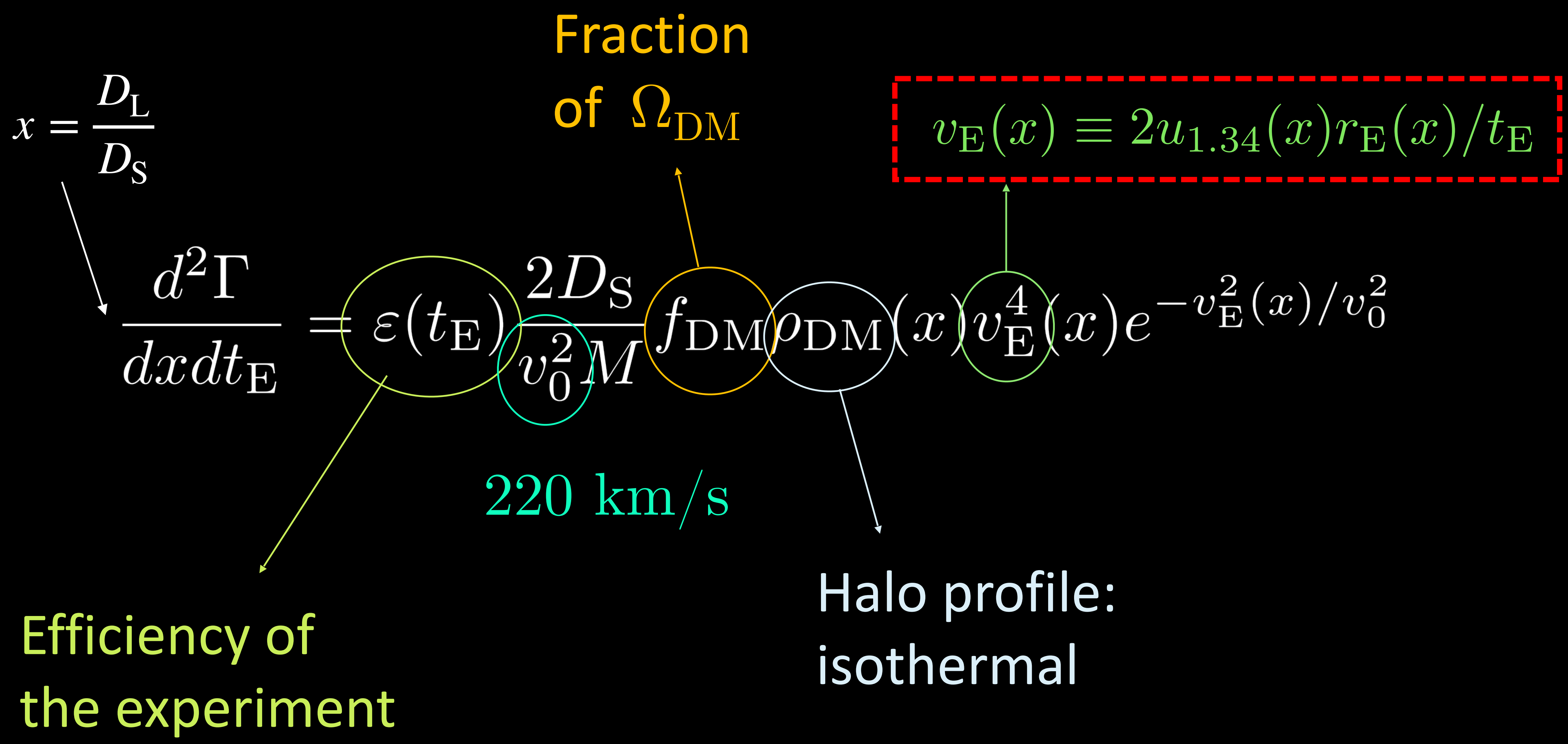

Fraction of Ω_{DM}

$$\boxed{v_{\mathrm{E}}(x) \equiv 2u_{1.34}(x) r_{\mathrm{E}}(x)/t_{\mathrm{E}}}$$

$$x = \frac{D_{\mathrm{L}}}{D_{\mathrm{S}}}$$

$$\frac{d^2\Gamma}{dx\,dt_{\mathrm{E}}} = \varepsilon(t_{\mathrm{E}})\frac{2D_{\mathrm{S}}}{v_0^2 M} f_{\mathrm{DM}}\rho_{\mathrm{DM}}(x) v_{\mathrm{E}}^4(x) e^{-v_{\mathrm{E}}^2(x)/v_0^2}$$

$220\ \mathrm{km/s}$

Efficiency of
the experiment

Halo profile:
isothermal

Constraining extended objects

The total number of expected events depends on the experiment

$$N_{\text{events}} = N_\star T_{\text{obs}} \int_0^1 dx \int_{t_{\text{E,min}}}^{t_{\text{E,max}}} dt_{\text{E}} \frac{d^2\Gamma}{dx dt_{\text{E}}}$$

Constraining extended objects

The total number of expected events depends on the experiment

$$N_{\rm events} = N_\star T_{\rm obs} \int_0^1 dx \int_{t_{\rm E,min}}^{t_{\rm E,max}} dt_{\rm E} \frac{d^2\Gamma}{dx\, dt_{\rm E}}$$

Number of observed stars

EROS-2 LMC: 5.49×10^6

OGLE-IV: 4.88×10^7

Observation time

EROS-2 LMC: 2500 days

OGLE-IV: 1826 days

Constraining extended objects

The total number of expected events depends on the experiment

$$N_{\rm events} = \boxed{N_\star}\, \boxed{T_{\rm obs}} \int_0^1 dx \boxed{\int_{t_{\rm E,min}}^{t_{\rm E,max}}} dt_{\rm E} \frac{d^2\Gamma}{dx\, dt_{\rm E}}$$

Maximum and minimum transit time

Number of observed stars

Observation time

EROS-2 LMC: 2500 days

OGLE-IV: 1826 days

EROS-2 LMC: 5.49×10^6

OGLE-IV: 4.88×10^7

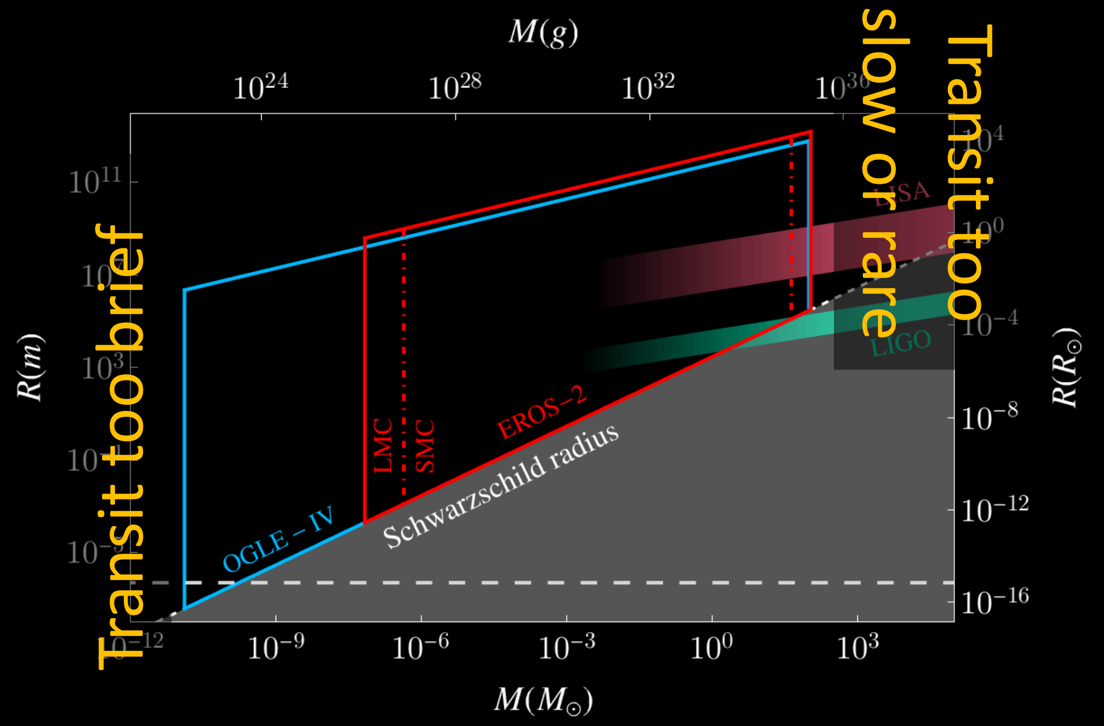

Transit too brief

slow or rare

Transit too

Obtaining constraints

To obtain limits, we have to account for the observed events

- EROS-2: 3.9 events at 90% CL
- OGLE-IV: $\mathcal{O}(1000)$ astrophysical events, Poissonian 90% CL: $\kappa = 4.61$

$$N_i^{\mathrm{SIG}} \equiv N_i^{\mathrm{FG}} + N_i^{\mathrm{DM}}$$

Bin events in $\mathrm{t_E}$

$$\kappa = 2 \sum_{i=1}^{N_{\mathrm{bins}}} \left[N_i^{\mathrm{FG}} - N_i^{\mathrm{SIG}} + N_i^{\mathrm{SIG}} \ln \frac{N_i^{\mathrm{SIG}}}{N_i^{\mathrm{FG}}} \right]$$

Lensing geometry

- Up to this point, we have assumed that the sources are point-like light sources (a good approximation for EROS/OGLE)
- This approximation breaks down when $r_E = \theta_E D_L \sim r_S$
- Geometry in the lens plane:

$r_s \equiv xR_\star / r_E$

$$\bar{u}(\varphi) = \sqrt{u^2 + r_S^2 + 2ur_S \cos\varphi}$$

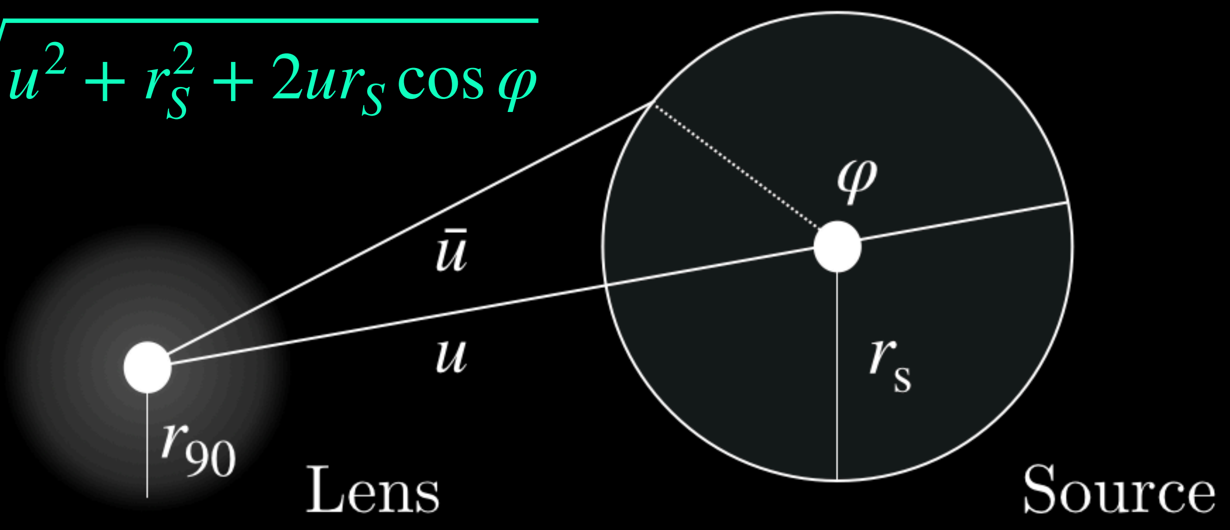

Lensing equation:

$$\bar{u}(\varphi) = \tau(\varphi) - \frac{m(\tau(\varphi))}{\tau(\varphi)}$$

Image

Image

$$\mu_i = \eta \frac{1}{\pi r_S^2} \int_0^{2\pi} d\varphi \, \frac{1}{2} \tau_i^2(\varphi)$$

Star sizes in M31

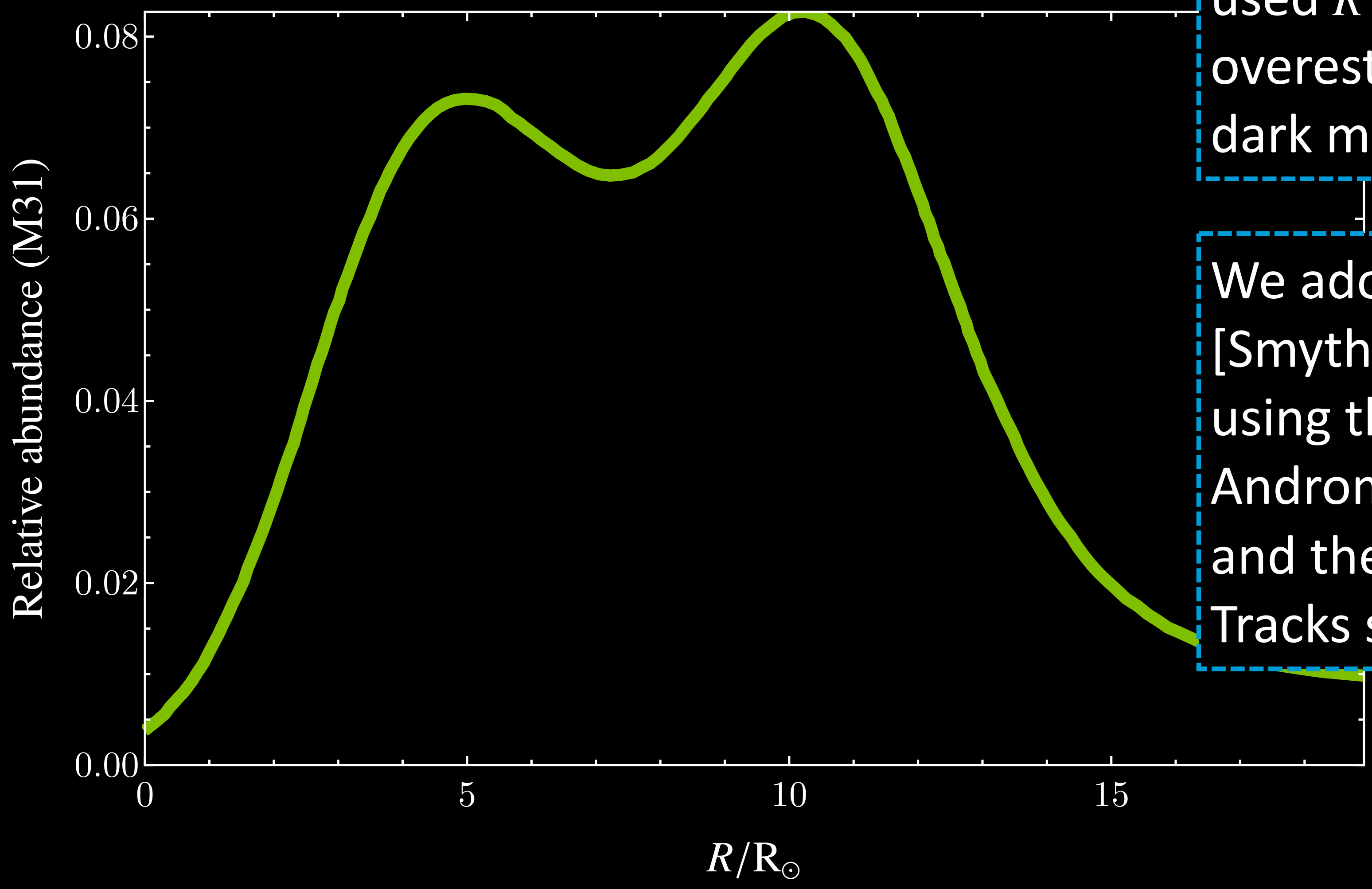

Initially, the Subaru-HSC collaboration used $R = \mathrm{R}_\odot$ for all stars, but this overestimates the constraints on the dark matter fraction

We adopt the distribution derived in [Smyth et al., PRD, arXiv:1910.01285] using the Panchromatic Hubble Andromeda Treasury star catalogue and the `MESA` Isochrones and Stellar Tracks stellar evolution package

$$N_{\text{events}} = N_\star T_{\text{obs}} \int dt_{\mathrm{E}} \int dR_\star \int_0^1 dx \frac{d^2\Gamma}{dx\,dt_{\mathrm{E}}} \frac{dn}{dR_\star}$$

Feature importance

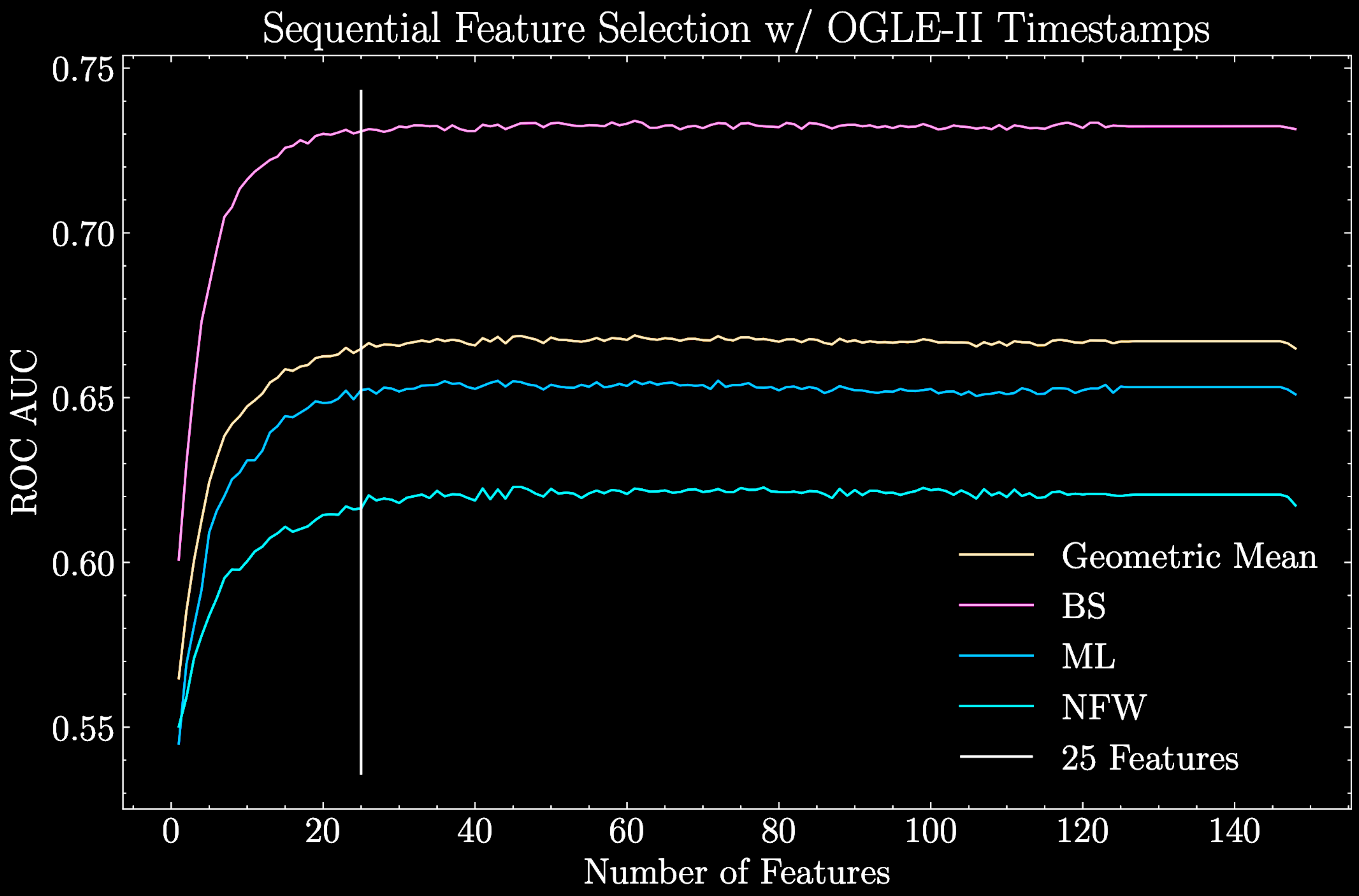

Opportunities for positive detection

Miguel Crispim-Romao, DC, arXiv:2402.00107

Caustics arise for $0.8 < \tau_m < 3$